remote sensing

MDPI

Article

Spatiotemporal Variation of Hourly Scale Extreme Rainstorms in the Huang-Huai-Hai Plain and Its Impact on NDVI

Huiting Zuo [1], Yunsheng Lou [2,3,*] and Zhongliang Li [4]

[1] School of Applied Meteorology, Nanjing University of Information Science &Technology, Nanjing 210044, China; 20151112060@nuist.edu.cn
[2] Collaborative Innovation Center on Forecast and Evaluation of Meteorological Disasters, School of Applied Meteorology, Nanjing University of Information Science and Technology, Nanjing 210044, China
[3] Jiangsu Key Laboratory of Agricultural Meteorology, Nanjing University of Information Science and Technology, Nanjing 210044, China
[4] College of Computer and Software, Nanjing Vocational University of Industry Technology, Nanjing 210046, China; 2021101228@niit.edu.cn
* Correspondence: yslou@nuist.edu.cn; Tel.: +86-13770338381

Abstract: This paper utilizes high-resolution ERA5 hourly data from 1980 to 2020 and long-term normalized difference vegetation index (NDVI) time series obtained from remote sensing and applies trend analysis, correlation analysis, lag analysis, and other methods to study the spatiotemporal characteristics of extreme rainfall at daily and hourly scales in the Huang-Huai-Hai Plain. The paper explores the NDVI's variability and its relationship with extreme hourly precipitation and analyzes the main factors affecting it. The study made the following observations: (1) The extreme daily precipitation in the Huang-Huai-Hai Plain shows a decreasing trend, with a 13.6 mm/yr reduction rate. In contrast, the proportion of extreme rainfall to total precipitation generally exceeds 20%, and the intensity of extreme rain has gradually increased. The spatial distribution pattern of extreme rainfall follows the distribution pattern of China's rain belts, with the terrain being an important influencing factor. The high-incidence areas for extreme rainfall are the Huaihe River region and the Shandong Peninsula. (2) The observed significant increase in hourly extreme precipitation events in the Shandong and Henan provinces of the Huang-Huai-Hai Plain has led to an increased risk of flooding, while the corresponding events in the northwest region of the Plain have exhibited a gradual weakening trend over time. (3) The extreme hourly precipitation in the Huang-Huai-Hai plain shows a frequent and scattered pattern, with decreasing intensity over time. Extreme precipitation mainly occurs in the first half of the night, especially between 19:00 and 21:00, with extreme hourly rainfall intensity fluctuating between 0.2 and 0.25 and the proportion of rainfall to total precipitation reaching as high as 10%. The spatial distribution of extreme hourly rainstorms during the peak period (19:00–21:00) exhibits a high rainfall volume, intensity, and frequency pattern in the eastern region, while the western part exhibits low rainfall volume, intensity, and frequency. (4) The incidence of extremely heavy rainfall in an hour has exhibited a more significant increase compared to extreme daily events in the Huang-Huai-Hai Plain, primarily in the form of backward-type precipitation. Hourly extreme precipitation events in the Huang-Huai-Hai Plain are affected by terrain and land use/cover change (LUCC), with the micro-topography of hilly areas leading to a concentrated distribution of precipitation and LUCC suppressing extreme precipitation events in arid climates. (5) At the ten-day scale, the spatial distribution of the NDVI shows a gradually increasing trend from northwest to southeast, with the highest NDVI value reaching up to 0.6 in the southern part of the study area. For extreme hourly precipitation, there is no significant change observed at the multi-year ten-day scale; while the NDVI in the northern and central parts of the Huang-Huai-Hai Plain shows a significant decreasing trend, in contrast, it presents a significant increasing trend in the southern region. (6) Finally, the correlation between NDVI at the ten-day scale and extreme hourly precipitation exhibits a decreasing pattern from north to south, with a correlation coefficient decreasing from 0.48 to 0.08. The lagged correlation analysis of extreme hourly rainfall and NDVI for one, two, and three ten-day periods shows that the lagged effect of extreme hourly precipitation on NDVI is negligible. Analyzing the correlation between extreme hourly rainfall and

Citation: Zuo, H.; Lou, Y.; Li, Z. Spatiotemporal Variation of Hourly Scale Extreme Rainstorms in the Huang-Huai-Hai Plain and Its Impact on NDVI. *Remote Sens.* **2023**, *15*, 2778. https://doi.org/10.3390/rs15112778

Academic Editor: Seon Ki Park

Received: 8 April 2023
Revised: 5 May 2023
Accepted: 8 May 2023
Published: 26 May 2023

NDVI for different months, the impact of extreme hourly precipitation on NDVI is predominantly negative, except for June, which shows a positive correlation (0.35), passing the significance test. This study offers a scientific foundation for enhancing disaster warning accuracy and timeliness and strengthening the research on disaster reduction techniques.

Keywords: NDVI; extreme hourly precipitation; extreme daily precipitation; rainfall type; topography; land use and land cover change

1. Introduction

The intensification of global warming has been progressively leading to more severe and recurrent extreme weather events [1]. Extreme weather events are strongly inclined towards amplification in magnitude, frequency, and probability [2–6]. As a consequence of climate change, there is a rise in the number of extreme weather incidents involving heavy rain and precipitation. The destructive effects of these events encompass floods, landslides, and endangerment to human lives, infrastructure, farms, and ecological systems [7]. Moreover, climate change is responsible for the modification of rain patterns, which in turn results in fluctuations in both the frequency and intensity of rain occurrences; however, increased precipitation does not always increase total annual or seasonal rain—it just occurs during more intense events [8]. Significant regional disparities in precipitation and economic development make China highly vulnerable to extreme rainfall [9,10]. For instance, based on data from the International Disaster Database, in 2010 alone, the losses caused by hydrological disasters in China reached as high as USD 18.9 billion, representing 40% of the global total [11]. On 21 July 2012, a severe rainstorm struck Beijing, causing 79 fatalities and economic damages amounting to CNY 11.64 billion [12]. On 20 July 2021, a devastating rainstorm hit Zhengzhou, resulting in 398 deaths and numerous people reported missing, while causing direct economic damages totaling CNY 120.6 billion [10]. Therefore, a reasonable assessment of extreme precipitation's spatial and temporal characteristics, such as frequency, intensity, and variability, is essential for predicting future rainstorms and upgrading disaster emergency response measures.

The study revealed an escalating tendency in the overall pattern of extreme daily precipitation in China [13–18]. Observations from most meteorological stations indicate an increase in the length of excessive precipitation periods, with earlier start dates and later end dates [19]. The IPCC report demonstrates that precipitation's temporal and spatial distribution also changes due to global warming. The topography and wetness vary significantly in different regions, with extreme rainfall exhibiting high regional complexity and spatiotemporal variability [20–23]. The research uncovered a fascinating trend: a noticeable decline in extreme precipitation events in the northern, central, and northeastern areas of China over time. Simultaneously, there has been a rise in these occurrences within the northwestern, southwestern, and Yangtze River regions. This shift in extreme precipitation events highlights the complex interplay of various factors and underscores the need for further investigation and adaptation strategies in response to these changing patterns [24–27]. These regional differences are caused by insufficient moisture availability on land, natural climate variability, and dynamic changes.

In addition, studies have found that the most significant increases were for extreme precipitation events, which could reach 99.8% or 99.9% on the sub-daily scale [28–31], emphasizing the importance of using sub-daily scale observations. The intensification rate of short-term extreme precipitation (sub-daily extreme precipitation) has exceeded that of extreme daily precipitation [32–35], mainly due to the release of latent heat, triggering short-term convective rainfall [36]. The characteristics of sub-daily extreme precipitation are significantly different from those of daily-scale rainfall, and the degree of disaster it causes far exceeds that of daily-scale rain [37]. The magnitude of the tragedies is much higher than that of daily-scale events [38].

The Huang-Huai-Hai Plain falls under the influence of the East Asian monsoon system and varies across different climatic regions. Due to significant changes in monsoon climate, unique terrain distribution, the wide span of land, and complex terrain, floods caused by extreme precipitation in summer have brought considerable losses to the economy and human life [39–41]. Most of the past studies conducted on the Huang-Huai-Hai Plain were based primarily on data related to daily precipitation, focusing on inter-decadal, long-term trends or primarily on extreme precipitation with a duration of 1 day or more. The hydrological consequences of excessive rainfall are influenced by various factors, among which the time of the precipitation event plays a crucial role. For example, short-term rain (on an hourly scale) is often caused by convective storms, which can lead to flash floods. Multi-day extreme rainfall is usually considered to be the leading cause of large-scale floods [42,43].

The study suggests that the most pronounced increases in extreme precipitation events may happen at sub-daily scales, potentially resulting in more frequent and intense flash floods [44]. Compared to extreme precipitation events lasting several hours, daily-scale and multi-day-scale extreme precipitation cannot accurately reflect the frequency and intensity of excessive rainfall, nor can they capture many details of the precipitation process [45,46]. Additionally, extreme precipitation at sub-daily time scales can exacerbate flood events [47,48]. Therefore, studying the robust precipitation characteristics of sub-daily time scales in the H-Plain region is necessary. The spatial heterogeneity of the H-Plain's surface morphology may result in complex regional-scale features of extreme hourly precipitation. Areas with complex geography usually experience rapid changes in extreme hourly precipitation from occurrence to peak [49].

During the examination of data related to extreme precipitation events, a multitude of research has employed various data sources. These consist of satellite remote sensing data (for example, TRMM, GPM, and IMERG), meteorological station observational data (including surface precipitation, temperature, and humidity), and climate reanalysis data (such as ERA-Interim, NCEP/NCAR, and ERA5 reanalysis data). By utilizing these diverse data sources, researchers can gain a more in-depth understanding of extreme precipitation events and develop more accurate predictive models [50–52]. These data sources feature different temporal and spatial resolutions, enabling researchers to analyze extreme precipitation events from multiple perspectives [53]. For instance, satellite remote sensing data provide continuous precipitation monitoring on a global scale, suitable for long-time series and large-area research. In contrast, meteorological station observation data offer high-temporal-resolution precipitation information, facilitating the hourly capture of extreme precipitation events [54]. Simultaneously, climate reanalysis data provide more complete and consistent climate background information for research, contributing to the analysis of the association between extreme precipitation events and atmospheric circulation [55]. Regarding the methods for processing and analyzing extreme precipitation events, standard methods include the sliding window method, the climate index method, empirical orthogonal function analysis (EOF), fluctuation analysis (such as wavelet analysis), and machine learning [56–58]. Utilizing these approaches, scientists are able to explore the spatiotemporal distribution features of extreme precipitation events and their connections to extensive climate factors (such as ENSO, AMO, and PDO) [59]. By applying the sliding window technique and EOF analysis, the spatiotemporal fluctuation traits of extreme precipitation occurrences in Northeast China and their association with climate oscillations have been uncovered. In recent years, machine learning methods in extreme precipitation event research have become increasingly widespread, such as predicting the occurrence probability of extreme precipitation events using random forest models [47].

Researchers employ multi-source data with different spatiotemporal resolutions when analyzing extreme precipitation events, providing abundant information for their study. In terms of processing and analysis methods, the sliding window method, climate index method, empirical orthogonal function analysis, fluctuation analysis, and machine learning methods are widely applied, helping to reveal the spatiotemporal features of

extreme precipitation events and their associations with large-scale climate factors. These comprehensive methods strongly support the study of extreme precipitation events and their impacts.

Due to economic growth and population concentration, the Huang-Huai-Hai Plain, a vital agricultural region in China, has experienced significant changes in its ecological environment. Extreme rainstorms affect agricultural production and threaten the region's social stability and ecological security. Severe rainstorms are closely related to local flooding and the environmental climate, and the mechanism behind extreme rainstorms is not precise. Extreme precipitation events can cause significant disasters once they occur. Consequently, investigating extreme precipitation in the H-Plain holds tremendous significance for facilitating the region's high-quality development. It can help reveal the causes and evolution of heavy rain and improve the accuracy and timeliness of disaster warnings. Investigating the interplay between intense precipitation at sub-daily timescales and climate change and anthropogenic activities in the H-Plain would offer a scientific foundation for both climate adaptation measures and sustainable development strategies. This paper employs ERA5 data with an hourly resolution to examine alterations in patterns of extreme precipitation at the sub-daily scale and identify the key factors that contribute to extreme precipitation's occurrence. Additionally, it examines the factors behind the spatiotemporal variations in severe rainstorms at the sub-daily time scale. The specific issues addressed are as follows:

(1) The spatiotemporal features of excessive rainfall at hourly intervals are analyzed in the H-Plain.
(2) The spatiotemporal differences between extreme hourly and daily precipitation in this study area are analyzed.
(3) The main influencing factors of excessive hourly heavy rain in the H-Plain are identified.

2. Materials and Methods

2.1. Overview of the Study Area

Situated in east-central China, the H-Plain is encircled by the northern Yanshan Mountains, the western Taihang Mountains, the eastern Bohai Sea and Yellow Sea, and the southern Huai River. It includes parts or all of Beijing, Tianjin, Hebei, Shandong, and Henan provinces and is a floodplain formed by intermittent floods of the Yellow, Huai, and Hai Rivers (see Figure 1). The H-Plain plays a crucial role as a grain cultivation region in China, producing summer corn and winter wheat. The region features a moderate monsoon climate, with an annual average temperature that varies between 8 and 15 °C; the mean annual precipitation is 734.9 mm [60]. The rain is primarily concentrated from July to September. The precipitation levels per year fall within the range of 500 to 1000 mm. Under the influence of the southeast monsoon, the area experiences a decline in available resources from southeast to northwest. Approximately 20–30% of these resources can be utilized for agricultural production, which falls short of fulfilling the demand for grain production. Therefore, a large amount of supplementary irrigation is still needed every year to ensure grain production [61].

2.2. Data Introduction

2.2.1. NDVI Data and Preprocessing

In this study, we aimed to process and combine NDVI data derived from two different remote sensing sources, namely, the AVHRR (Advanced Very High Resolution Radiometer) and the MODIS (Moderate Resolution Imaging Spectroradiometer). By merging the data from both sources, we successfully extended the time span of the dataset from 1982 to 2016, providing a comprehensive and consistent record of NDVI measurements for ecological and environmental research applications.

Data from AVHRR were procured from NASA's Goddard Space Center, extending from 1982 through 2010. Alternatively, MODIS surface reflectance information was collected from the Terra satellite's daily surface reflectance product, MOD09GA, formulated by NASA's MODIS terrestrial product division and spanning the years from 2010 to 2016.

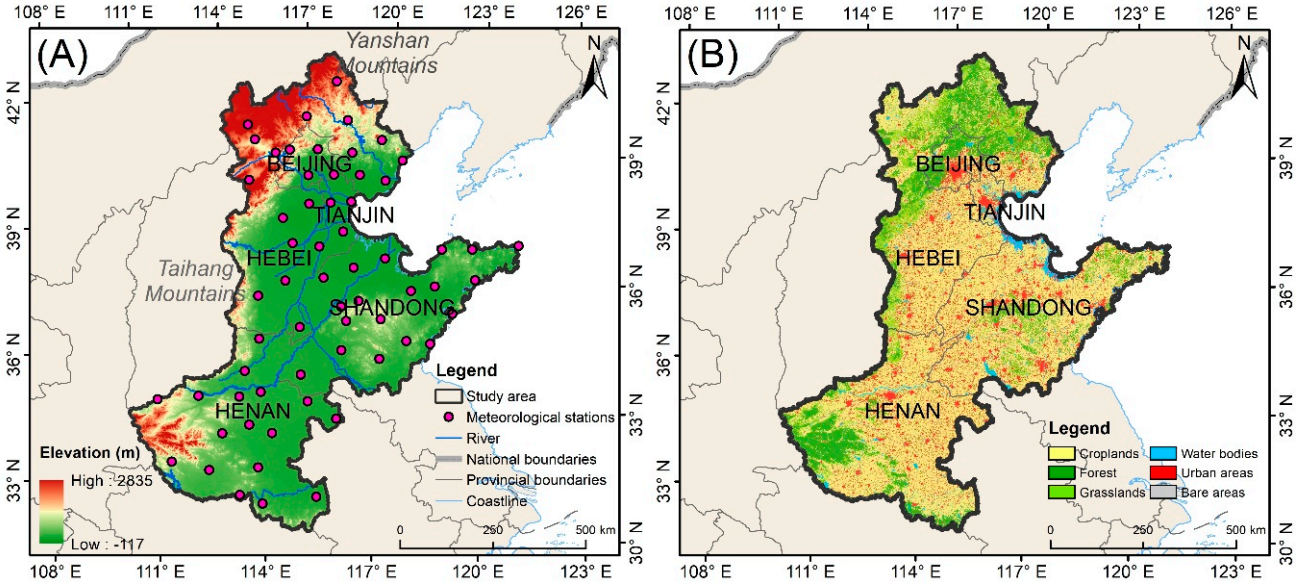

Figure 1. Overview of the natural features of study area. Note: Figure (**A**) shows the geographical overview of the H-Plain; Figure (**B**) shows the LUCC of the H-Plain.

To maintain the integrity and uniformity of the data, various processing methods were applied. For the AVHRR data, steps such as radiometric calibration, cloud identification and removal, atmospheric adjustment, satellite drift rectification, and bidirectional reflectance distribution function (BRDF) processing were executed. With regard to the MOD09GA data, quality assessment, image mosaic, subsetting, format and projection alteration, and other preprocessing tasks were carried out. These procedures were essential in acquiring a dependable and coherent NDVI dataset for subsequent examination.

In order to synthesize the daily data into monthly data, the Maximum Value Composites (MVC) technique was employed. This strategy allowed for the minimization of cloud or noise impacts present in the daily imagery, resulting in a more accurate representation of the vegetation dynamics over the entire study period.

2.2.2. Meteorological Data and Preprocessing

This article uses ERA5 hourly precipitation data to study extreme rainfall events at the hourly scale. The first step is to perform data quality control, including threshold value checking, outlier handling, and time consistency verification. Since ERA5 data may have trend bias in the frequency of heavy rainfall, data with strict quality control were used to quantify the possible trend bias [62,63]. In this study, the precipitation characteristics of ERA5 and ground meteorological station observation data from 1980 to 2018 were calculated and compared, with specific results shown in Figure 2. Due to the availability of hourly precipitation data, only a limited number of stations were selected to validate the ERA5 hourly data. A total of 16 observation stations (station numbers: 54038, 53399, 53599, 53697, 54618, 54499, 54416, 54525, 54526, 54627, 54846, 54929, 54812, 54997, 57075, 57188) were chosen, which uniformly cover the H-Plain region, verifying the scientific validity and feasibility of the ERA5 data. Although slight differences exist in the precipitation amounts described by the ERA5 data and ground observation data, the overall trend of precipitation change is consistent, indicating that the quality-controlled ERA5 hourly data exhibit good temporal consistency and coherence. Based on the above research, this paper uses ERA5 hourly data to study the extreme precipitation events at an hourly scale in the H-Plain region.

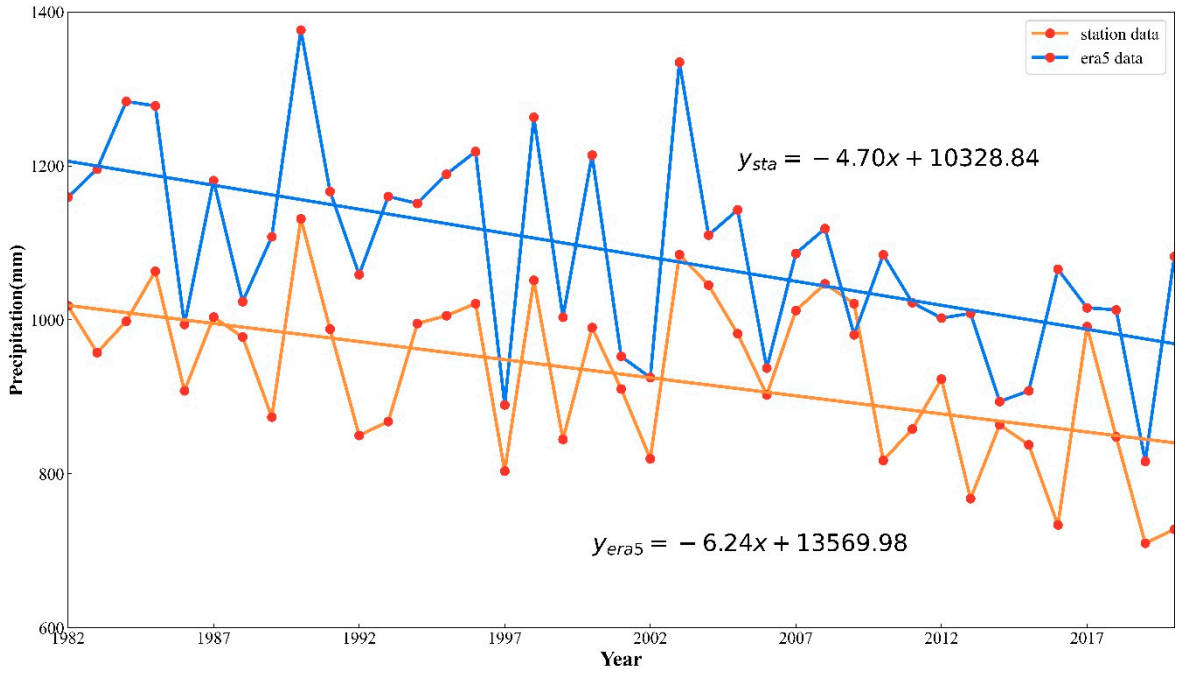

Figure 2. Comparison of ERA5 data and CMFD data for the H-Plain.

2.3. Methods

2.3.1. Extreme Precipitation Indices

This paper uses the percentile method [64] to establish the extreme precipitation thresholds for various time scales. All daily precipitation samples (daily precipitation $\geq$ 0.1 mm) were sorted in ascending order, and the threshold for daily extreme precipitation was determined by taking the value at the 95th percentile (R95daily). Similarly, all hourly precipitation samples (daily precipitation $\geq$ 0.1 mm) were sorted in ascending order, and the threshold for hourly extreme precipitation was established by using the value at the 95th percentile (R95hourly). These thresholds are used to determine eight precipitation indices that describe extreme precipitation patterns at various time scales. Please refer to Table 1 for the definitions and detailed descriptions of the eight indices.

Table 1. Delineation of extreme precipitation indices.

Precipitation Index	Definition	Unit
Precipitation (tp)	The cumulative precipitation exceeding 0.1 mm	mm
Daily rainstorm amount (tp_daily)	Daily precipitation $\geq$ R95daily	mm
Hourly rainstorm amount (tp_hourly)	Hourly precipitation $\geq$ R95hourly	mm
Contribution of rainstorm	The ratio of the sum of precipitation above the rainstorm threshold to the total amount of precipitation during the same period	dimensionless
Contribution rate of heavy rainfall area (contribution of area)	The ratio of the area where precipitation above the rainstorm threshold occurs to the total area where precipitation occurs within the same period	dimensionless
Frequency of rainstorm (frequency)	Frequency of rainstorms	dimensionless
Rainstorm intensity (intensity)	The ratio of cumulative precipitation surpassing a particular threshold to the duration of precipitation meeting or exceeding that threshold during the same period	mm/day or mm/hour
Rainstorm dispersion (cv)	The ratio of the standard deviation of intense rainfall to its corresponding average during the same period	dimensionless

2.3.2. Sen's Slope Estimation

Sen's slope technique offers substantial benefits over basic linear regression when analyzing trends in time series data. This method effectively mitigates the effects of outliers on the slope, does not necessitate a normal distribution for the time series, and accommodates outliers and missing values. Sen's slope is frequently employed in meteorological, remote sensing, and ecological/environmental studies to examine time series data trends. Formula: Sen's slope calculation can be expressed as follows:

$$\beta = \text{Median}\left(\frac{x_i - x_j}{i - j}\right) \quad (1)$$

Within the formula, "Median" represents the median function, and β illustrates the time series' evolving direction. When $\beta > 0$, it indicates an ascending trend, and a higher value denotes a more noticeable upward trajectory. Conversely, when $\beta < 0$, it indicates a descending trend, with a lower value signifying a more apparent decline.

2.3.3. Mann–Kendall (M-K) Test Method

The M-K test is an effective method for examining trends and abrupt changes in time series data. It does not necessitate particular sample distributions, is less affected by outliers, and offers a simple computation process. The steps for performing the M-K test are as follows:

$$S_k = \sum_{i=1}^{k} r_i \quad (k = 2, 3, \ldots, n) \quad (2)$$

Assuming random independence in time series, the statistical parameter is defined as follows:

$$UF_k = \frac{[s_k - E(s_k)]}{\sqrt{Var(s_k)}} \ (k = 1, 2, \ldots, n) \quad (3)$$

where $UF_1 = 0$, $E(s_k)$ and $Var(s_k)$ are the mean and variance of the cumulative sum of S_k and can be calculated from the following equation when $x_1, x_2, \ldots, x_n$ are mutually independent and have the same continuous distribution:

$$E(s_k) = \frac{n(n+1)}{4} \quad (4)$$

$$Var(s_k) = \frac{n(n+1)(2n+5)}{72} \quad (5)$$

2.3.4. Maximum Value Composites

The Maximum Value Composite (MVC) concept was introduced by Holben [65]. The particular equation for MVC [54] can be expressed as:

$$NDVI_i = Max(NDVI_{ij}) \quad (6)$$

where $NDVI_i$ denotes the *NDVI* in the *i*th month or the *i*th year and $NDVI_{ij}$ represents the *NDVI* data on the *j*th day in the *i*th month or on the *j*th month in the *i*th year.

3. Results

3.1. Spatiotemporal Characteristics of Extreme Daily Rainstorms

Figure 3 demonstrates that the precipitation levels in H-Plain follow a trend of steady increase from north to south, with both extreme daily rainfall and the proportion of extreme daily rainfall contribution showing a similar pattern. The maximum values of average precipitation and excessive rain appear in the southern part of Henan province. In contrast, The minimum values are situated in Hebei province's northern region. The Huaihe River region receives the most rainfall due to its location on the windward slope of the Dabie

Mountains and the fact that the Huaihe River belongs to the temperate monsoon climate zone, where the southeast monsoon from the ocean brings abundant rainfall.

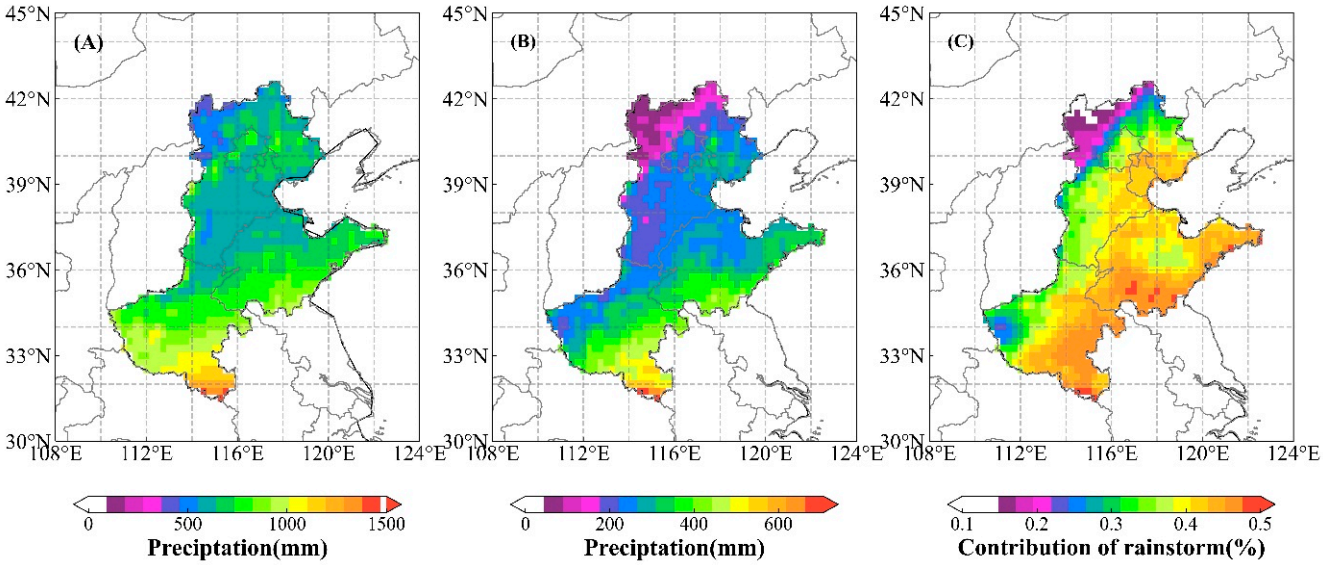

Figure 3. Spatial properties of severe daily rainfall in the H-Plain. Note: Figure (**A**) shows the average precipitation; Figure (**B**) represents the average value of multi-year extreme rainstorms (mean R95daily); Figure (**C**) depicts the ratio of heavy rainfall to overall precipitation.

Distinctive droughts and floods in Shandong province are attributed to the notable influence of the Pacific subtropical high-pressure system, where the proportion of extremely heavy rainfall makes up a significant portion of the total rainfall, reaching up to 50%. Meanwhile, the northern foothills of the Taihang Mountains have the greatest terrain fluctuations but have the least amount of daily rainstorms and the smallest proportion of daily rainstorms to total annual rainfall. The research findings indicate that the spatial distribution pattern of extreme daily precipitation in the study area is consistent with China's rain belt distribution pattern. This implies that the region is subject to similar weather patterns and has comparable susceptibility to extreme precipitation events as other areas within the rain belt. The terrain is a critical determinant. The high-incidence areas of excessive daily rainfall are the Huaihe River and the Shandong Peninsula.

Figure 4 presents the characteristics of the temporal variation in extreme daily precipitation within the H-Plain. From 1980 through 2020, extreme rainfall experienced substantial inter-annual fluctuations, and there was a significant decreasing trend observed in the annual amount of extreme rainfall, with a yearly reduction rate of 13.6 mm (A). This suggests that the region is experiencing a decline in the frequency and intensity of extreme precipitation events. The contribution rate of extreme rainfall has shown a stable trend over the years, remaining almost unchanged (B), accompanied by a consistently high contribution rate that surpasses 20% on average, and in some years, up to 50%; the annual variation amplitude was large. The contribution rate of extreme rainfall area, on the other hand, showed a rapid decrease (C). This suggests a decline in the incidence of heavy rainfall, while at the same time, there is an upsurge in the severity of excessive rainstorm events.

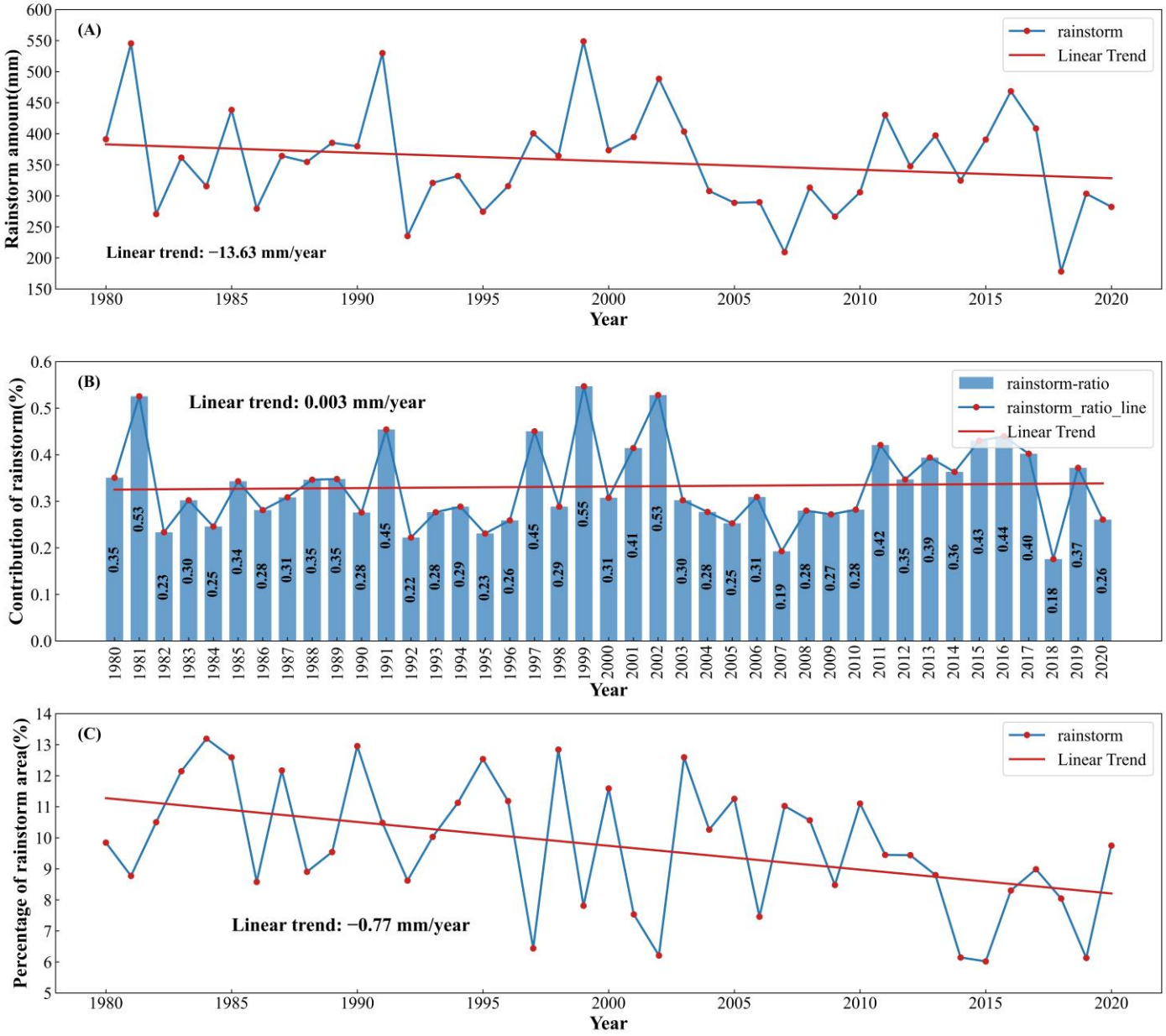

Figure 4. Characteristics of the multi-year average daily extreme rainfall, the proportion of heavy rain, and the proportion of rich rainfall area in the H-Plain. Note: Figure (**A**) illustrates the yearly sum of precipitation; Figure (**B**) shows the contribution rate of rainfall; Figure (**C**) shows the proportion of the area where rainfall occurs to the total area.

Figure 5 presents the statistical properties of the daily extreme precipitation sequence in the H-Plain covering the period from 1980 to 2020. During this period, the frequency of severe rainstorms shows a rapidly declining trend (A), with a significant inter-annual variation. The intensity of extreme rainstorms remains unchanged (B), while the dispersion of rainstorms decreased slowly over 40 years (C).

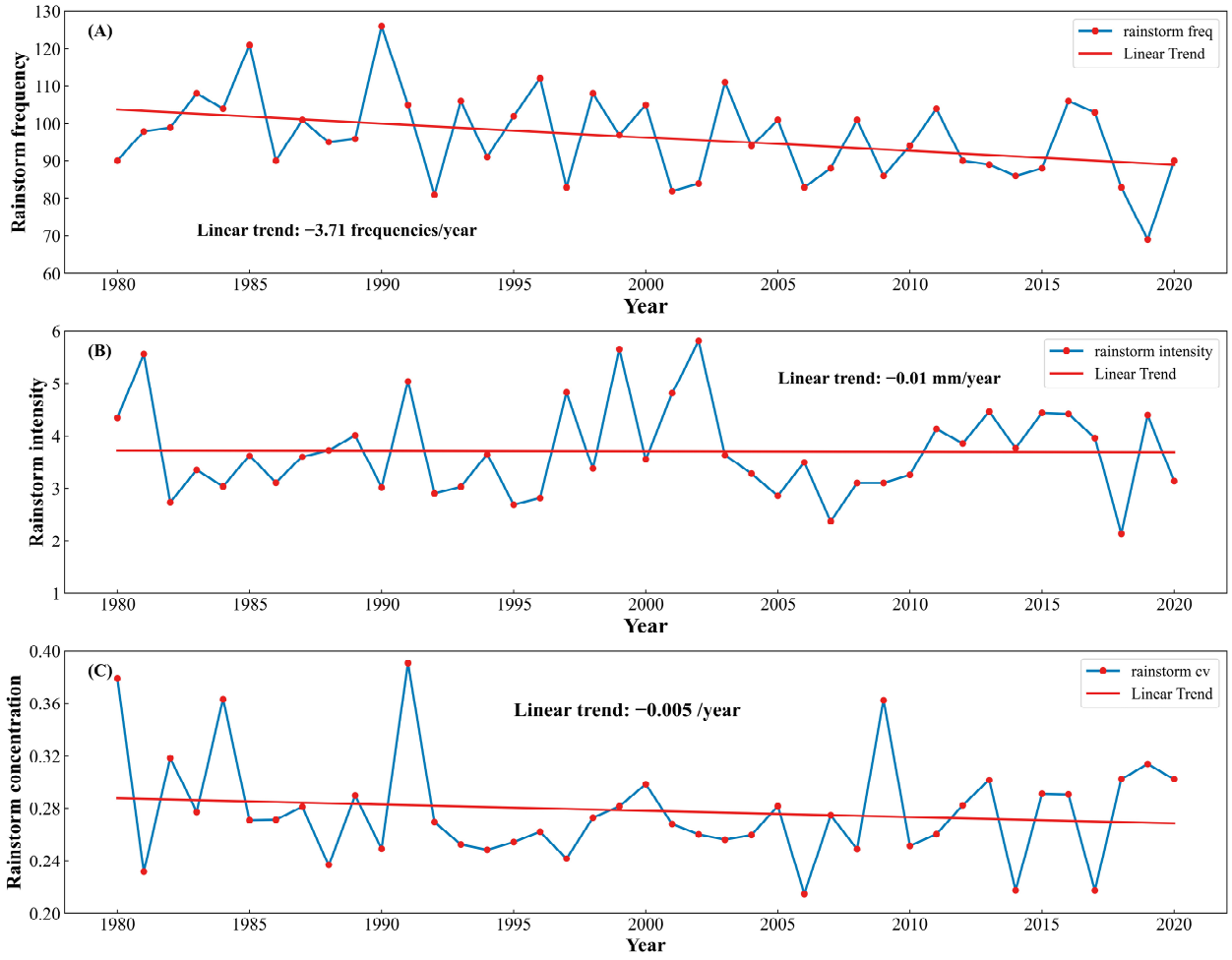

Figure 5. Frequency, intensity, and dispersion characteristics of daily extreme rainfall in the H-Plain. Note: Figure (**A**) represents the frequency of extreme rainfall events per year; Figure (**B**) illustrates the yearly intensity of extreme rainfall occurrences; Figure (**C**) depicts the yearly dispersion of such events.

3.2. Investigation into the Spatial and Temporal Features of Extreme Hourly Rainstorms

Figure 6 presents the spatial distribution characteristics of extreme hourly precipitation in the H-Plain from multiple perspectives. Figure 6A illustrates the intensity of extreme hourly rainfall, showing an overall increasing trend from west to east. The northwest region of the H-Plain, located on the leeward slope of the Taihang Mountains, exhibits the lowest intensity of extreme hourly rainfall, followed by Henan Province, with relatively low intensity. In contrast, Shandong Province experiences the highest precipitation intensity. Figure 6B displays the contribution rate of extreme hourly precipitation, demonstrating an increasing pattern from west to east. The northwest and southwest regions show lower contribution rates, while the Shandong Peninsula exhibits a high contribution rate of extreme precipitation. These findings collectively indicate that Shandong Province experiences significantly higher extreme precipitation events than other regions of the H-Plain. Figure 6C represents the concentration degree of extreme hourly precipitation, with the coastal areas of the Shandong Peninsula showing the highest concentration. Generally, there is an increasing spatial differentiation trend from northwest to southeast. Figure 6D shows the frequency of extreme hourly precipitation, which exhibits a similar pattern to the concentration degree, with higher frequency gradually increasing from northwest to southeast. The areas surrounding the Taihang Mountains have the fewest occurrences of extreme hourly rainfall, while the eastern part of the H-Plain experiences a higher frequency.

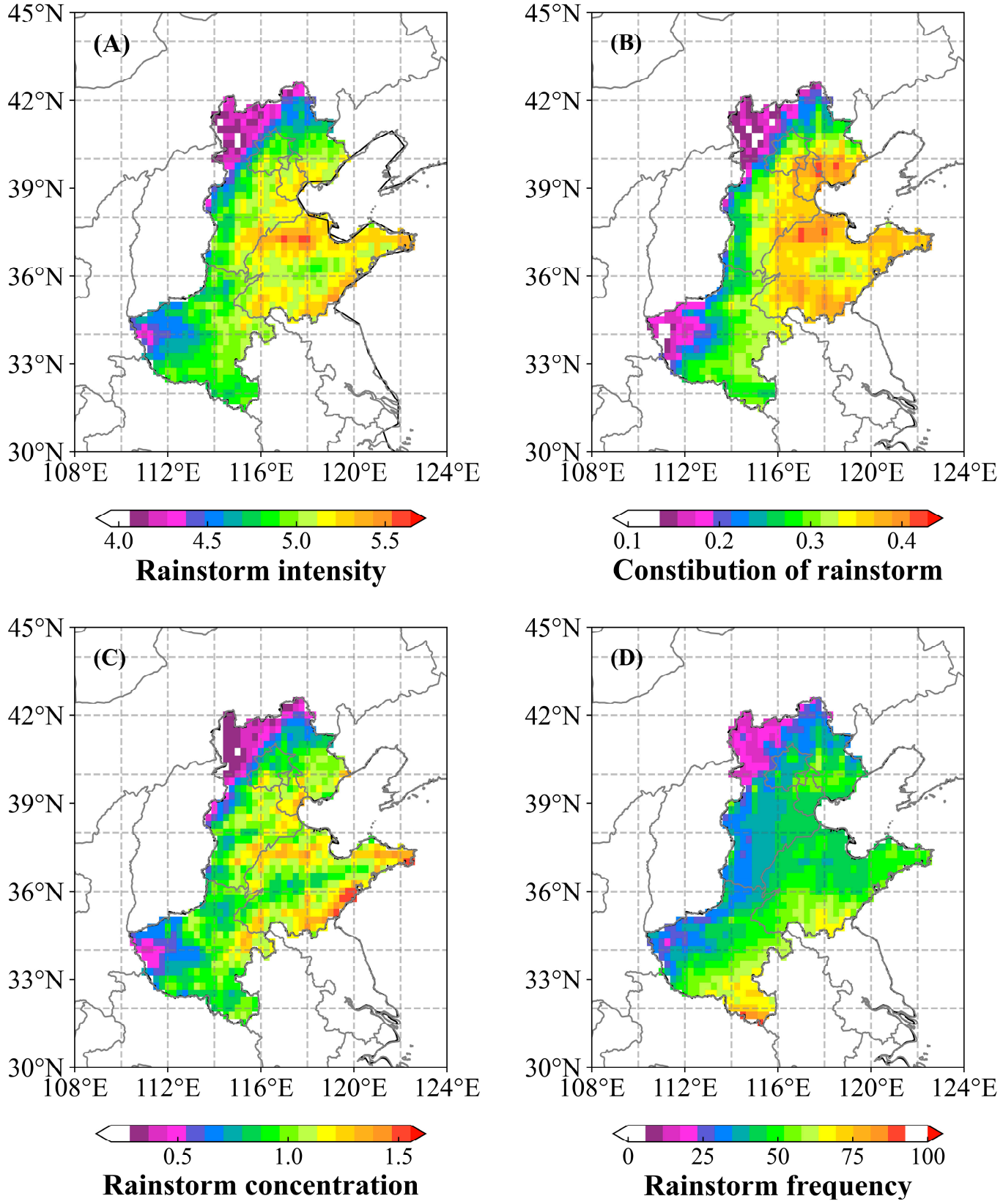

Figure 6. Characteristics of extreme hourly rainstorms in the H-Plain in terms of spatial distribution. Note: Figure (**A**) displays the magnitude of intense hourly rainfall; Figure (**B**) presents the percentage contribution of intense hourly rainfall, which is the proportion of extreme hourly rain compared to the total rainfall; Figure (**C**) displays the dispersion of intense hourly rainfall; Figure (**D**) shows the frequency of excessive hourly rainfall.

The characteristics of extreme precipitation on an hourly basis over many years are depicted in Figure 7. The frequency, intensity, and contribution rate of extreme hourly precipitation show significant changes at different times, with relatively stable values before 19:00 and reaching their peaks between 19:00 and 21:00. It can be deduced that extreme hourly precipitation is more likely to occur during nighttime (dominated by the first half of the night), which is completely different from the characteristics of extreme daily precipitation [66].

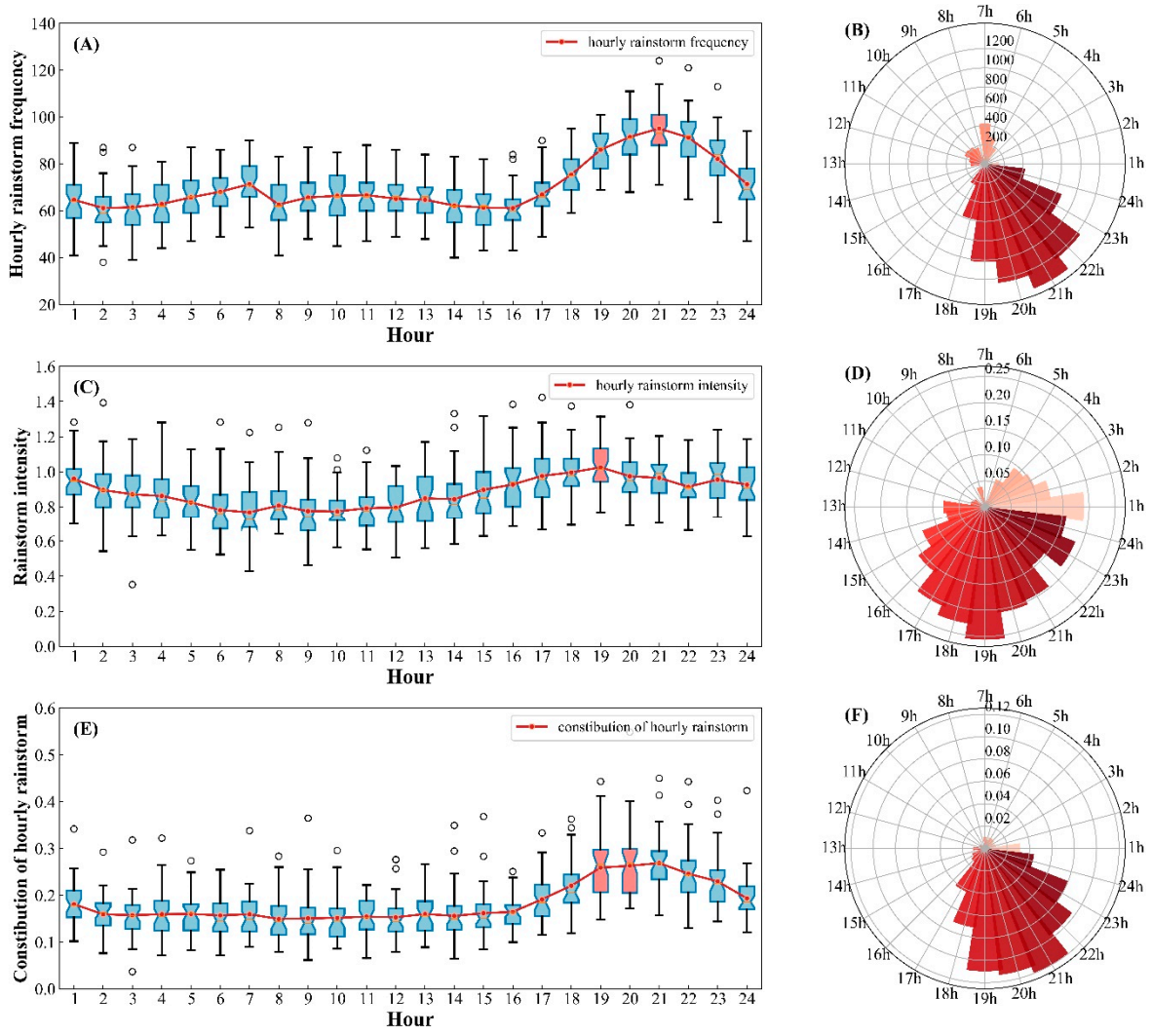

Figure 7. Temporal characteristics of extreme hourly rainstorms in the H-Plain. Note: (**A**) displays the frequency of extreme precipitation per hour; (**B**) shows the distribution of extreme precipitation frequency in a radial pattern; (**C**) presents the intensity of hourly extreme precipitation; (**D**) shows the radial distribution of hourly extreme precipitation intensity; (**E**) illustrates the proportion of extreme hourly precipitation relative to the overall precipitation; (**F**) shows the radial distribution of extreme hourly precipitation as a proportion of the total precipitation.

Figure 8 illustrates the time-related features of extreme hourly rainfall in the H-Plain over the last 40 years. The intensity (Figure 8A), frequency (Figure 8D), and dispersion (Figure 8G) of extreme hourly rainfall have all exhibited a significantly decreasing trend at the annual scale, with dispersion decreasing the fastest, suggesting that extreme rainfall events have become more dispersed, resulting in a decline in associated risks. In terms of seasonality, excessive hourly rainfall exhibits the most incredible intensity, frequency, and dispersion during summer, whereas the opposite holds true during winter. The monthly variation in extreme rainfall intensity, frequency, and dispersal is most significant in July,

indicating that severe summer rainfall hazards are the greatest. The intensity of powerful rainfall per hour displays diverse features on various time scales, with a declining tendency regarding annual ranking and a notable upward trend for the monthly scale. Although summer is the season with the highest strength for extreme hourly rainfall, it displays a decreasing trend. Similarly, the frequency and dispersion of excessive hourly rainfall also exhibit similar tendencies on both annual and monthly scales, but extreme hourly rain in summer is significantly higher. In contrast, the dispersion of excessive hourly rainfall shows a decreasing trend. In summary, it can be seen that extreme hourly rainfall shows a characteristic of frequent and dispersed occurrence, and its intensity is decreasing.

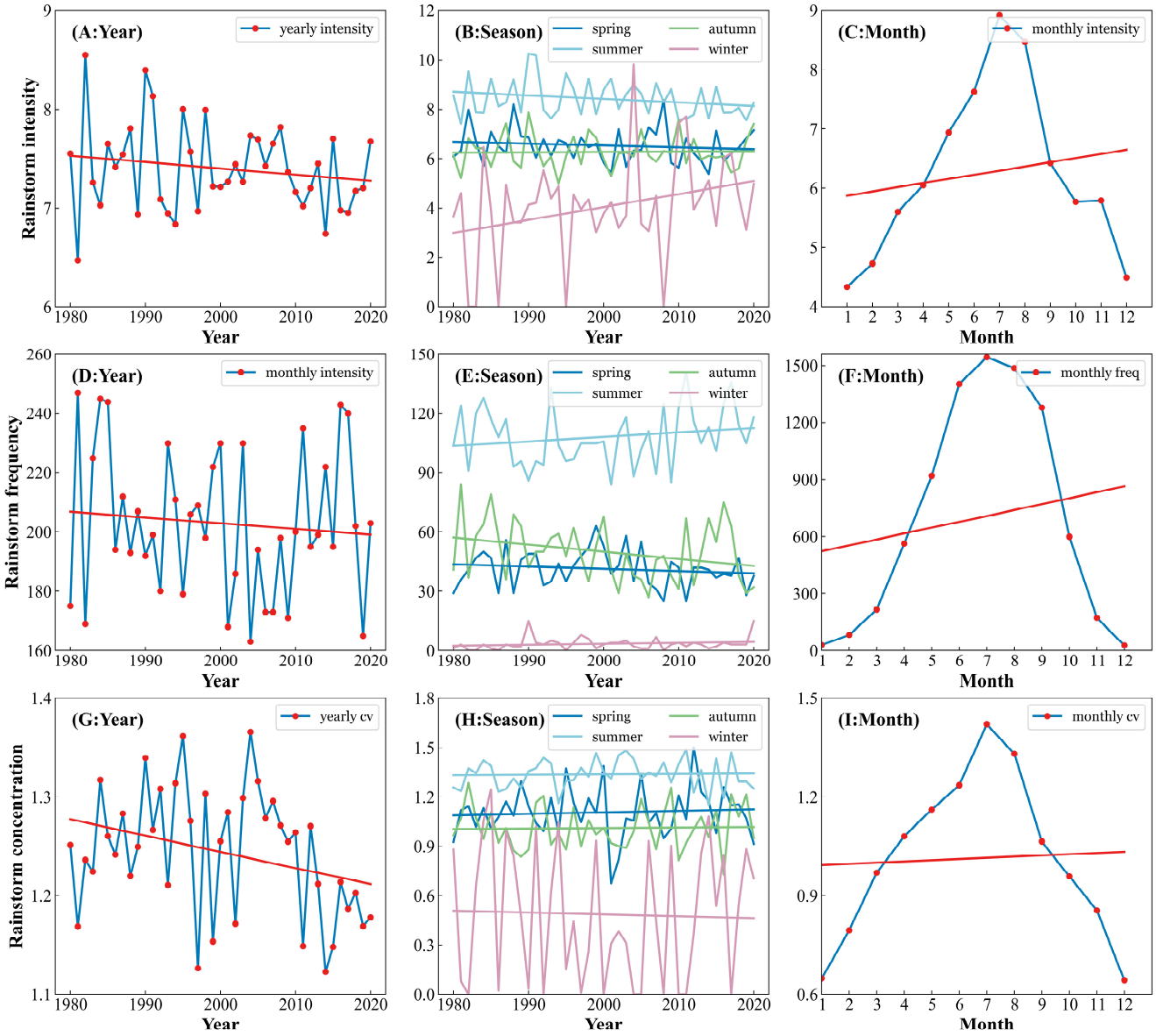

Figure 8. Multi-timescale characteristics of extreme hourly rainstorms in the H-Plain. Note: (**A**) shows the annual variation in hourly extreme rainfall intensity; (**B**) shows the seasonal variation in hourly extreme rainfall intensity; (**C**) shows the monthly variation in hourly extreme rainfall intensity; (**D**) illustrates the interannual variability of extreme hourly rainfall frequency; (**E**) depicts the fluctuations in the frequency of severe hourly precipitation across various seasons; (**F**) illustrates the fluctuations in hourly extreme rainfall frequency monthly; (**G**) illustrates the changes in hourly extreme rainfall dispersion throughout the year; (**H**) illustrates the seasonal fluctuations in dispersion in extreme hourly rainfall; (**I**) demonstrates the monthly variation in dispersion in extreme hourly rainfall.

Figure 9 illustrates the geographical features of severe hourly precipitation during two particular periods (19:00 and 21:00, which exhibit the maximum frequency and intensity) in the H-Plain. The typical geographical spatial distribution of intense rainfall indicates that the eastern region receives a greater amount of rainfall with higher intensity and frequency. The western region has less rain and lower power and frequency. Despite the low precipitation and weaker intensity, the northern region exhibits a significant contribution to extreme precipitation. At the same time, the western and southern parts of Henan Province and the Shandong Peninsula have high rainfall, intensity, proportion, and frequency, which are inextricably linked to the topography. The urban construction land in the northern part of Hebei Province has less rainfall and lower intensity, proportion, and frequency, indicating that urbanization specifically impacts extreme rainstorms in the region. In addition, the rain and frequency at 21:00 showed a decreasing trend compared with 19:00, indicating that the intense hourly rainstorms mainly occurred in the first half of the night.

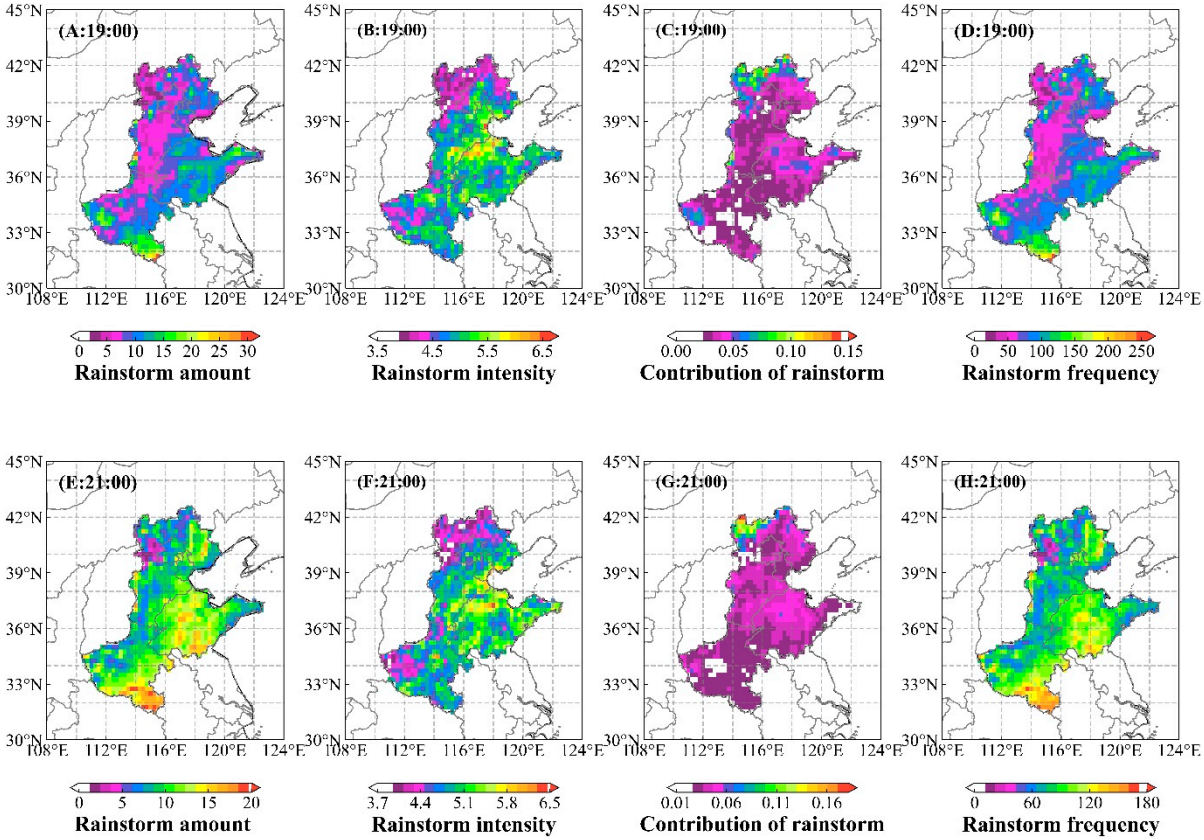

Figure 9. A comparative analysis is conducted to examine the spatial features of extreme hourly rainstorms at two specific time points (19:00 and 21:00) in the H-Plain. Note: Figure (**A**) illustrates the precipitation quantity of the extreme rainfall event occurring at 19:00; Figure (**B**) illustrates the intensity of extreme rainfall events at 19:00; Figure (**C**) illustrates the percentage of the total extreme rainfall amount that occurred at 19:00; Figure (**D**) depicts the frequency of extreme rainfall events at 19:00 in graphical form; Figure (**E**) illustrates the precipitation volume of the extreme rain event occurring at 21:00; Figure (**F**) displays the intensity of extreme precipitation at 21:00; Figure (**G**) displays the ratio of the amount of extreme rainfall at 21:00 to the overall amount of extreme rainfall; Figure (**H**) illustrates the occurrence rate of extreme rainfall incidents at 21:00.

3.3. Analysis of Extreme Hourly Rainstorm Extremes Characteristics

Over the past forty years, a declining tendency has been identified in the peak value of extreme hourly precipitation within the H-Plain region (Figure 10A), accompanied by significant inter-annual variations, primarily oscillating between 20 and 45 mm. The fre-

quency of occurrence of the maximum value of extreme hourly rainfall shows a decreasing trend from 1:00 to 24:00 (Figure 10B), and the overall trend can be divided into three time periods: 1:00–7:00, 8:00–19:00, and 20:00–24:00; extreme hourly rainfall shows an increasing trend within each period.

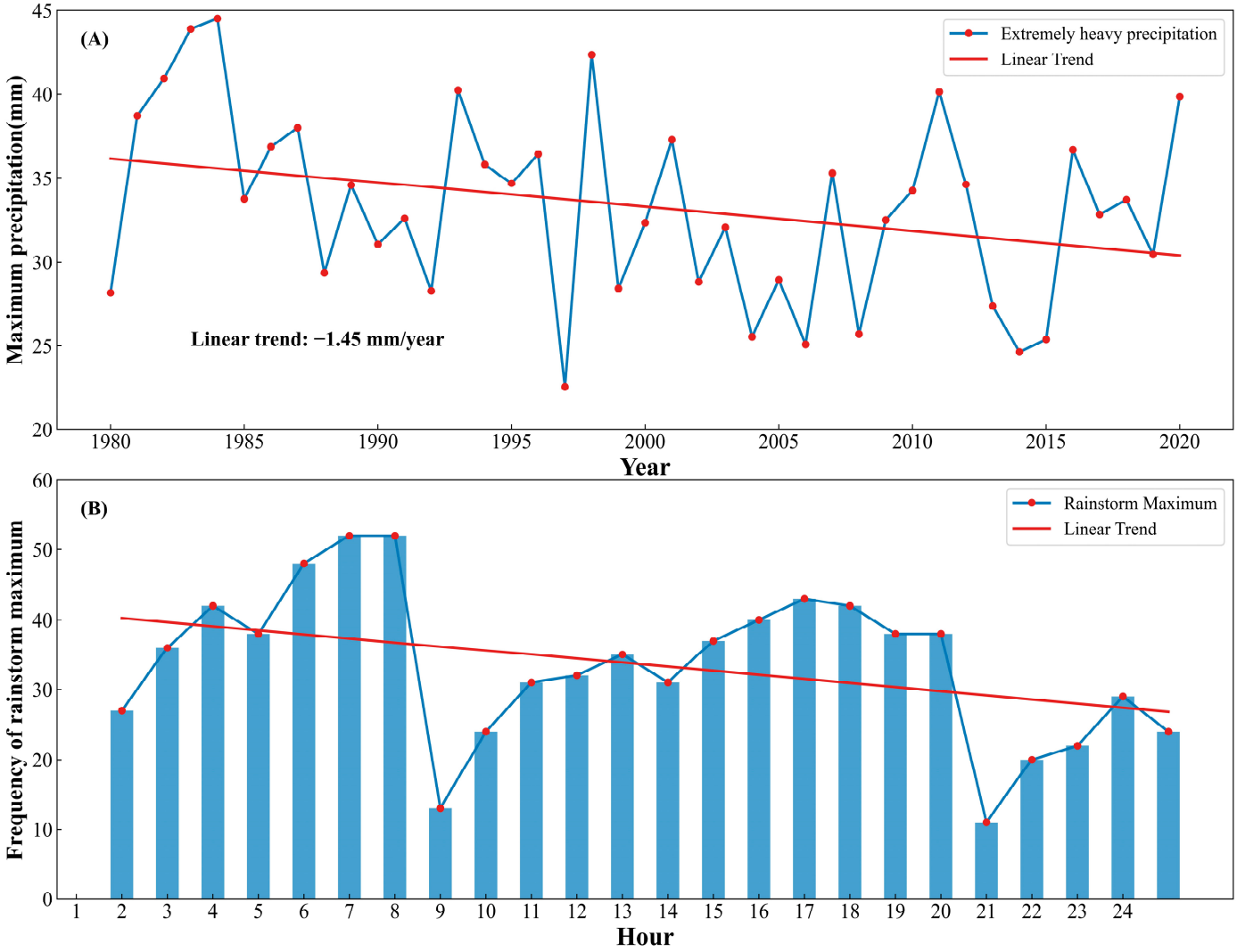

Figure 10. Extreme characteristics of extreme hourly rainstorms in the H-Plain. Note: Figure (**A**) shows the annual maximum value of extreme hourly rainfall, and Figure (**B**) illustrates the frequency of the maximum value of extreme rainfall on an hourly basis.

For the past 40 years, trailing-type precipitation has been the predominant form of heavy rainfall in the H-Plain, with occasional balanced-type precipitation and bimodal precipitation and rare single-day-type precipitation (Figure 11A). This suggests that the precipitation is more concentrated and that the extreme precipitation characteristics at hourly scales should be paid more attention to. According to Figure 11B, the trailing-type precipitation occurs most frequently, indicating that the local rain has a fat-tail distribution. The extreme hourly values of extremely heavy rainfall mainly happen in the first half of the night. Although 2000 was recognized as a pivotal moment for climate change [55], the rainfall type did not change before or after this point.

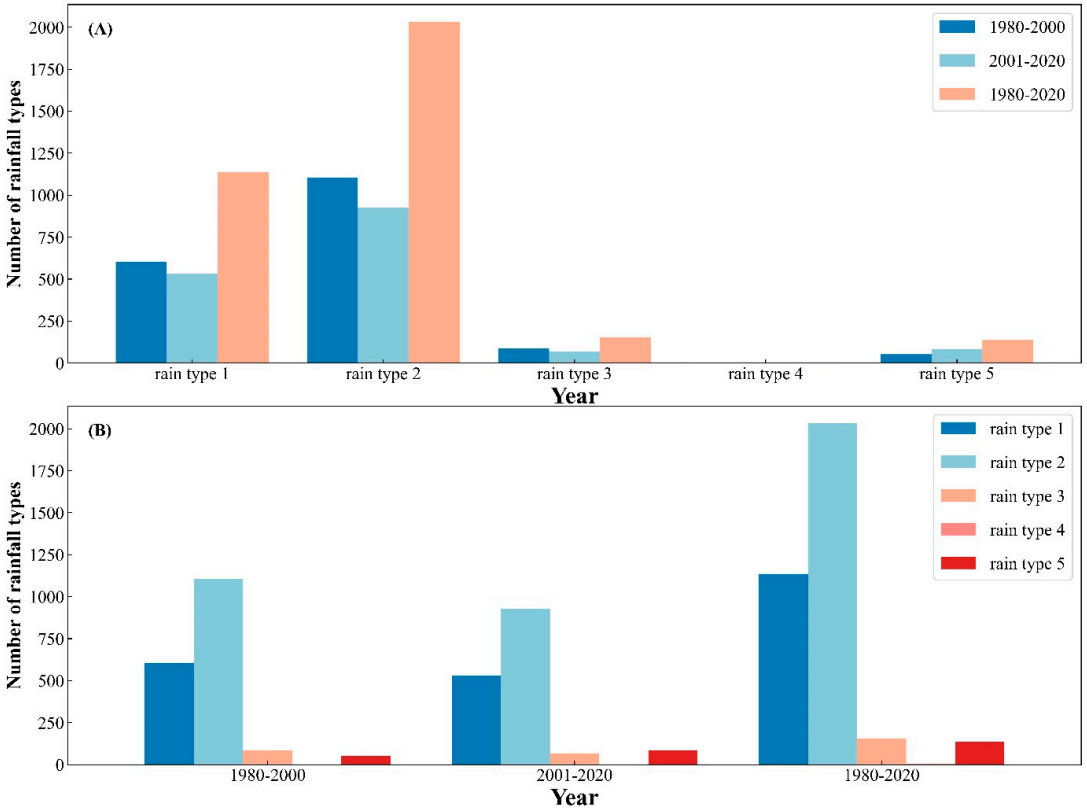

Figure 11. The characteristics of rainfall types in extreme rainstorms in the H-Plain. Note: Figure (**A**) presents the statistical distribution characteristics of five rainfall types across different decadal periods. Rain type 1 represents predominant precipitation; rain type 2 represents post-dominant precipitation; rain type 3 represents balanced precipitation; rain type 4 represents single-day precipitation; rain type 5 represents bimodal precipitation; Figure (**B**) shows the proportion of five rainfall types across different decadal periods. Rain type 1 represents predominant precipitation; rain type 2 represents post-dominant precipitation; rain type 3 represents balanced precipitation; rain type 4 represents single-day precipitation; rain type 5 represents bimodal precipitation.

3.4. The Impact of Extreme Hourly Precipitation on NDVI

Figure 12 displays the spatial distribution and variation trend characteristics of extreme hourly precipitation and NDVI at the ten-day scale in the Huang-Huai-Hai Plain region. The figure reveals that on a ten-day scale, the extreme hourly rainfall in the region exhibits a distinct spatial differentiation pattern, increasing from the northwest to the southeast. In particular, areas with higher elevations experience less extreme hourly precipitation at the ten-day scale. In contrast, regions such as the Shandong Peninsula and Henan exhibit substantial extreme hourly precipitation levels (Figure 12A). Based on the Sen's slope and Mann–Kendall (MK) test results, it can be observed that in the H-Plain region, there has been no significant change in the extreme hourly precipitation at the multi-year ten-day scale, as shown in Figure 12B. Correspondingly, the overall distribution of the NDVI at the ten-day scale also demonstrates an increasing trend from the northwest to the southeast. The northern part of the study area and some coastal regions exhibit lower NDVI values, and land-use types in areas with lower NDVI values are predominantly urban. In contrast, the southern part of the study area exhibits higher NDVI values, reaching up to approximately 0.6, indicating a favorable local ecological environment. This translation adheres to a rigorous and professional academic writing style. Figure 12D illustrates the local NDVI variation trends. In the northern and central parts of the H-Plain, the NDVI presents a significant decreasing trend, while in contrast, the southern region exhibits a significant increasing trend. As can be inferred from the figure, the overall trend of the NDVI in the H-Plain indicates environmental degradation.

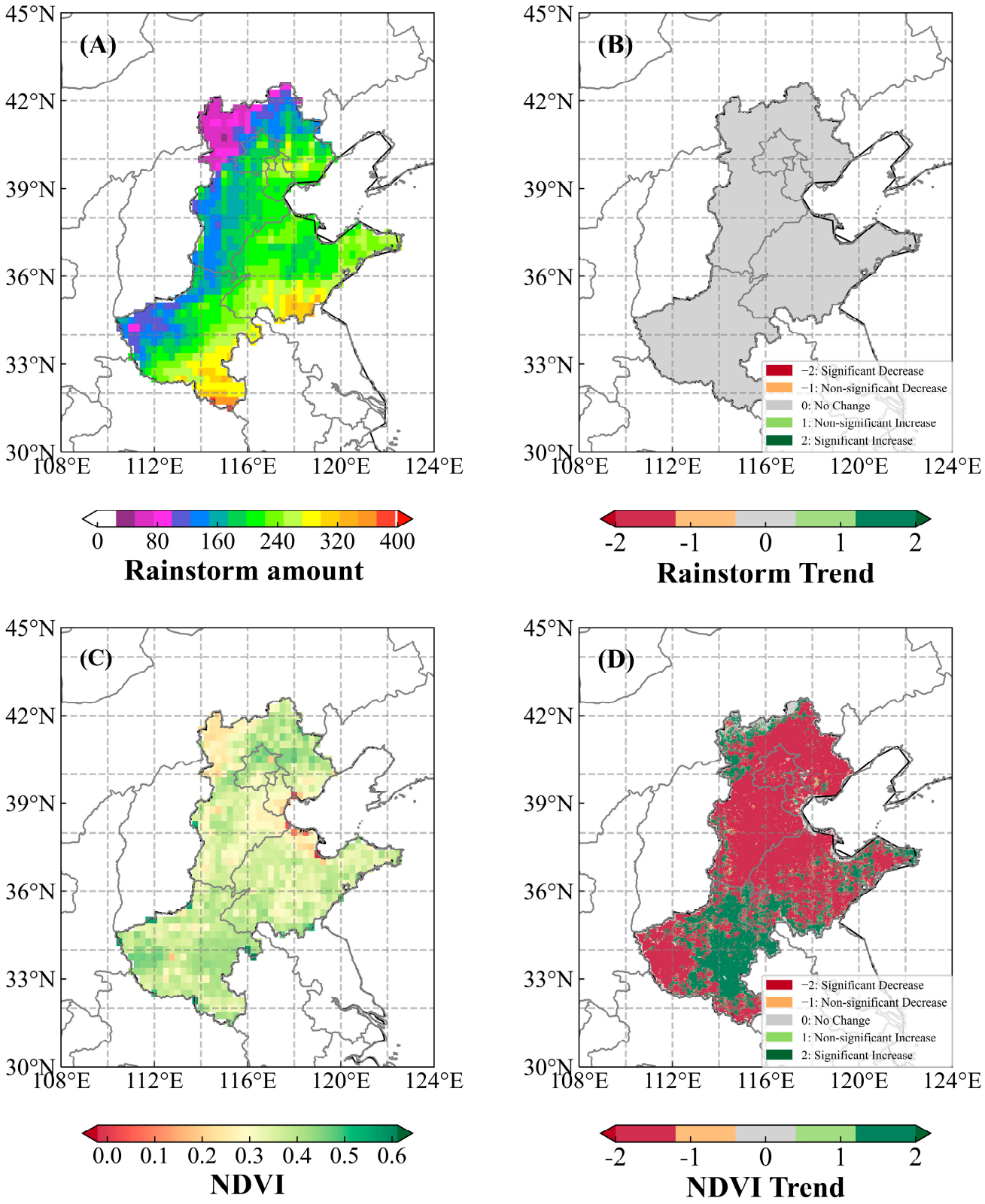

Figure 12. Trend analysis of extreme hourly rainfall and NDVI at ten-day scale in the H-Plain. Note: Figure (**A**) represents the spatial distribution characteristics of the multi-year average state of extreme hourly precipitation; Figure (**B**) depicts the spatial variation trend characteristics of extreme hourly precipitation; Figure (**C**) illustrates the spatial distribution characteristics of the multi-year average state of NDVI; and Figure (**D**) demonstrates the spatial variation trend characteristics of NDVI.

As shown in Figure 13, the correlation between extreme hourly precipitation at the ten-day scale and NDVI exhibits a distinct regional differentiation pattern characterized by a gradual decrease in the correlation coefficient from north to south. In the figure, only a few individual coastal areas in the Shandong Peninsula exhibit a non-significant relationship between extreme hourly precipitation and NDVI after conducting the significance test. Specifically, the correlation between extreme hourly precipitation and NDVI is relatively high in the northern part of the study area; it further decreases in the central part and is the lowest in the southern part. Additionally, lagged correlations of one, two, and three ten-day periods were analyzed for extreme hourly precipitation and NDVI, revealing that the lagged effect of extreme hourly precipitation on NDVI is negligible.

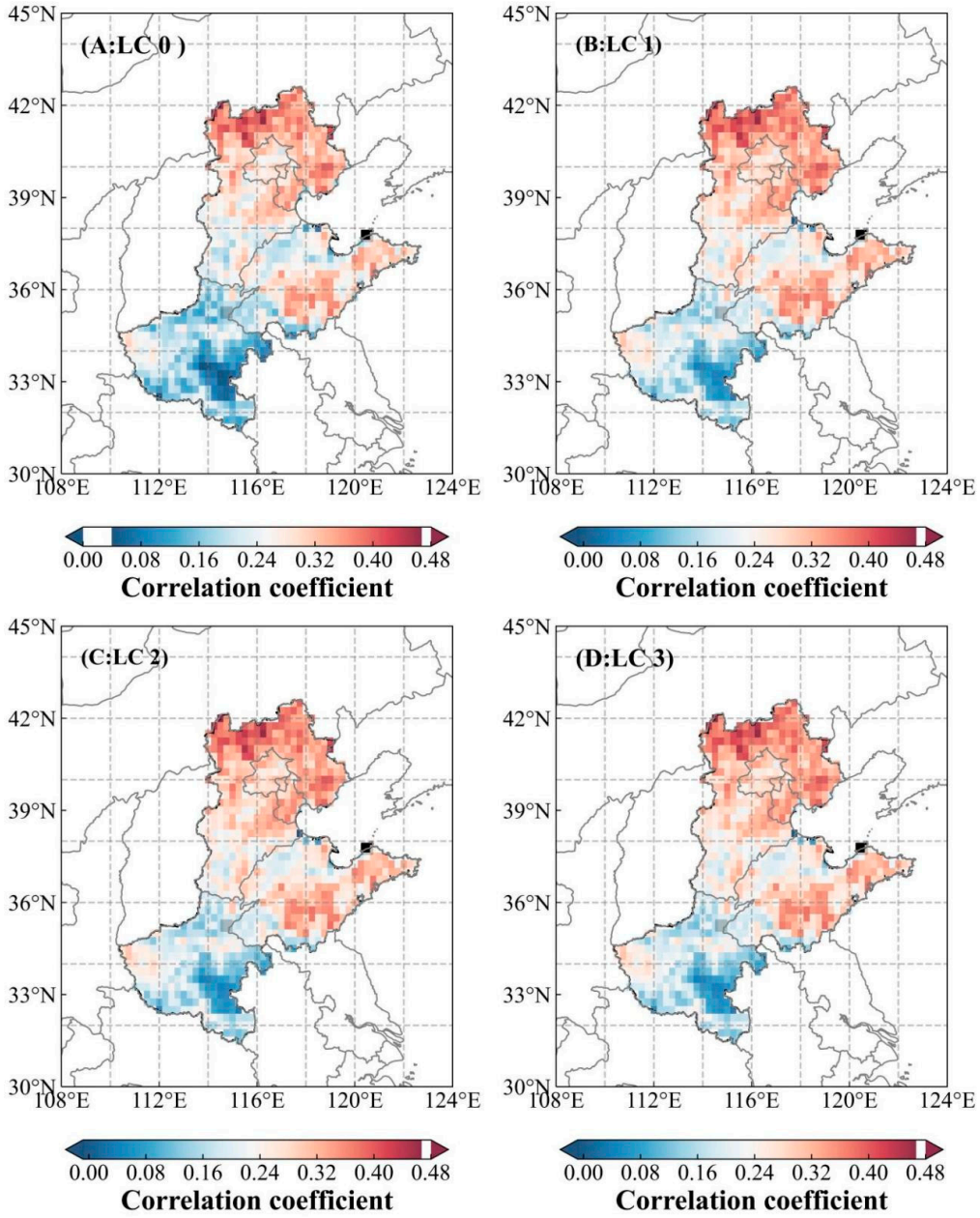

Figure 13. Decadal-scale extreme hourly rainstorm and NDVI correlation analysis in the H-Plain. Note: Figure (**A**) LC0 represents zero-lag correlation (no lag); Figure (**B**) LC1 represents first-order lag correlation; Figure (**C**) LC2 represents second-order lag correlation, and Figure (**D**) LC3 represents third-order lag correlation. The correlation coefficients in the figure are calculated under a significance level of 5%. Among them, the black squares denote markers that did not pass the significance test.

Owing to the delayed response of vegetation to climate variables, there exists a distinct lag effect in the relationship between NDVI and precipitation. Nevertheless, studies investigating the influence of extreme hourly precipitation on NDVI are scarce. Therefore, considering the instantaneous nature of excessive rainfall, this study calculates the correlation between NDVI and extreme hourly precipitation at the same time (LC0), extreme hourly precipitation lagged by one period (LC1), extreme hourly precipitation lagged by two periods (LC2), and extreme hourly precipitation lagged by three periods to analyze the lag effect of extreme hourly precipitation on NDVI. Combining Table 2 and Figure 14, The examination of the relationship between extreme hourly precipitation and NDVI across various months reveals that the effect of extreme hourly precipitation on NDVI is mainly negative. The correlations for March, June, and October are statistically significant at the $p < 0.05$ level. March and October show negative correlations, while June shows a positive correlation. As seen in Figure 14, extreme precipitation is relatively low in March, while vegetation has already begun to enter the growing season, characterized by a gradual increase in NDVI; the lack of rainfall may have inhibited vegetation growth. June is part of the rainy season, with substantial precipitation, and it coincides with summer; the lower NDVI may be due to the synergistic effect of temperature, but rainfall positively impacts NDVI during this time. In October, rain significantly decreases, but vegetation is still within the growing season; the reduction in precipitation has a suppressive effect on the NDVI.

Table 2. Correlation coefficients of monthly-scale extreme hourly rainstorms and NDVI.

Month	Correlation	*p*_Value	Significant
1	0.02	0.32	
2	−0.28	0.09	
3	−0.28	0.01	***
4	−0.02	0.21	
5	−0.01	0.54	
6	0.35	0.00	***
7	−0.08	0.11	
8	−0.01	0.32	
9	0.06	0.50	
10	−0.21	0.03	***
11	−0.23	0.12	
12	0.14	0.16	

Note: *** represents that the correlation coefficients have passed a significance test at a 95% confidence level, indicating statistical significance.

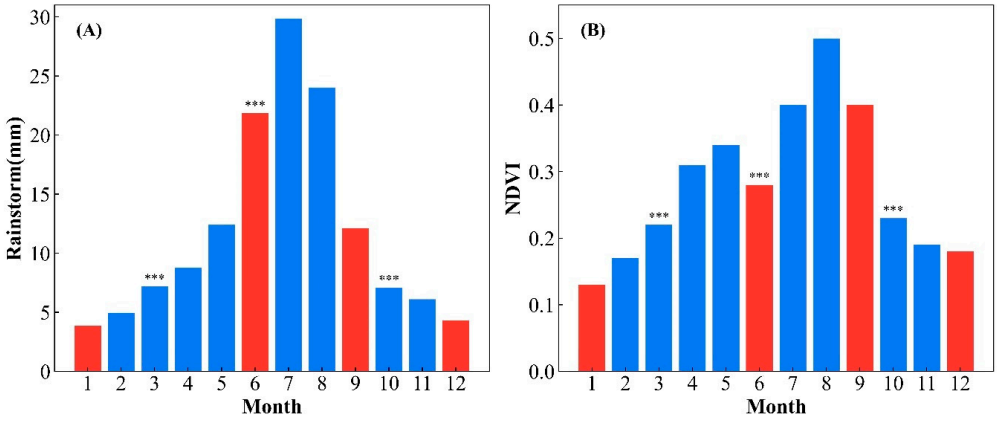

Figure 14. Correlation analysis of extreme hourly rainfall and NDVI at a monthly scale in the H-Plain. Note: Figure (**A**) represents the climatological mean of extreme hourly precipitation for each month over multiple years. The red color in the figure represents a positive correlation, while the blue color signifies a negative correlation, and the symbol [***] indicates that the significance test of $p < 0.05$ is passed. Figure (**B**) represents the average state of NDVI for each month over multiple years. The red color in the figure represents a positive correlation, while the blue color signifies a negative correlation, and the symbol [***] indicates that the significance test of $p < 0.05$ is passed.

4. Discussion

There are significant variations observed in the spatiotemporal distribution patterns of extreme rainfall events when comparing the daily and hourly scales in the H-Plain. The daily-scale extreme precipitation in this region is mainly distributed in summer. These events tend to have a long duration and a large spatial extent due to the influence of warm and humid airflow and convective activities [67–69]. On the other hand, extreme rainfall events at the hourly scale are more likely to occur during spring, summer, and autumn seasons and are often caused by cold fronts, convective activities, or low eddies, with short durations and smaller spatial extents. The H-Plain is particularly prone to extreme hourly rainfall during the rainy season and typhoon period. It is influenced by southwestern warm and humid airflows and southeastern cold air, forming complex weather systems and resulting in a higher frequency of extreme rainfall [70]. In the summer of the Shandong Peninsula, especially in June and July, extreme daily precipitation is more frequent, while heavy hourly rain occurs more frequently in August and September. The spatial and temporal distributions of excessive rainfall in the H-Plain are considerably impacted by the regional climate and weather systems at different time scales. Different meteorological systems and climate mechanisms mainly cause these temporal differences. Hourly-scale extreme rainstorm events are usually more dispersed in time, making them difficult to predict and monitor, while daily extreme precipitation events generally have higher spatial consistency and predictability.

The H-Plain region has been experiencing significant impacts from climate change factors, such as monsoon intensity, El Niño events, and atmospheric circulation, which have been observed to greatly affect extreme precipitation events [71,72]. The ecological environment of the H-Plain region is heavily influenced by several climatic factors, which also determine the frequency and intensity of extreme precipitation events in the area. The precipitation patterns in the region are greatly affected by monsoons, which bring increased water vapor during the summer months [73]. The intensity of the East Asian monsoon activity plays a significant role in the occurrence rates of extreme precipitation events [74], with studies indicating a positive correlation between monsoon strength and the likelihood of such events [75]. In addition to monsoons, El Niño events also have a significant impact on extreme precipitation events in the H-Plain region. These events lead to changes in precipitation patterns, which affect both the frequency and intensity of extreme precipitation events [76,77]. For instance, the 1998 El Niño event led to multiple floods and disasters in the region, illustrating the potential consequences of such climatic occurrences [78]. It is essential to comprehend and forecast El Niño occurrences to manage disasters effectively, given that they often result in heightened frequency and intensity of extreme precipitation events in the H-Plain region. Understanding the impact of El Niño events is crucial in preparing for potential floods and disasters in the region. The significance of predicting these events cannot be overstated, especially since they can have devastating consequences on the ecological environment and the people living in the region [79,80].

Changes in atmospheric circulation play a significant role in the development of extreme precipitation events in the H-Plain region. Anomalies in such events can be attributed to alterations in the transportation of water vapor by atmospheric circulation, which affects the precipitation processes in the area [81]. For instance, when the Northwest Pacific subtropical high is abnormally strong, the precipitation in the H-Plain region may increase significantly, triggering extreme precipitation events [82]. This demonstrates the importance of atmospheric circulation in shaping the region's precipitation patterns and the potential consequences of such changes. In light of these findings, future research plans to quantify the relationships between these climatic factors and extreme precipitation events, with the aim of more accurately assessing their contributions to extreme precipitation events in the H-Plain region. This knowledge will not only help to understand the underlying mechanisms driving extreme precipitation events but will also aid in developing more effective strategies for mitigating the ecological and environmental impacts of such events.

By exploring the complex interplay between monsoon intensity, El Niño events, and atmospheric circulation, researchers can develop a more comprehensive understanding of the H-Plain region's vulnerability to extreme precipitation events and work towards more resilient and adaptive strategies for managing the consequences of climate change. In conclusion, climate change factors such as monsoon intensity, El Niño events, and atmospheric circulation play a significant role in shaping extreme precipitation events in the H-Plain region. By better understanding these factors and their relationships with extreme precipitation events, researchers can more accurately assess their contributions and develop targeted strategies for mitigating the ecological and environmental impacts of such events in the region.

The distribution and intensity of extreme rainfall events can vary across different areas of the H-Plain due to various factors such as topography, land use patterns, and atmospheric conditions. This can result in spatial heterogeneities, where some areas experience more intense and frequent extreme rainfall events compared to others. The daily-scale severe rainstorm events in this region typically have a more comprehensive distribution range, especially in the plain areas where the daily-scale extreme precipitation is more uniformly distributed [83]. In contrast, hourly extreme rainfall events tend to occur in local areas, in mountainous or hilly regions. This is due to the complexity of the terrain and topography in these areas, leading to increased local precipitation and more concentrated hourly extreme rainfall [84]. The distribution of excessive rainfall at the daily scale is predominantly observed in the southern and western regions. In contrast, the hourly-scale extreme precipitation is primarily distributed in the northeast and central regions [85]. Due to warm and humid air currents, the occurrence and intensity of precipitation events is higher in the eastern and southern regions of the H-Plain. As a result, these areas are more prone to extreme weather conditions.

The northwestern and northern parts of the H-Plain tend to be drier, experiencing fewer instances of extreme precipitation. Such events are typically caused by large-scale weather systems that occur daily, such as typhoons and fronts, with a broader distribution. At the same time, hourly-scale excessive rainfall is usually caused by small-scale convective systems, such as convective cloud masses and thunderstorms with a smaller distribution [86]. For example, daily-scale extreme precipitation may be influenced mainly by air pressure and temperature. In contrast, hourly-scale extreme precipitation may be more influenced by convective layer structure and water vapor transport [87]. In addition, extreme precipitation can be distributed differently at various scales due to topography and land use factors [88,89].

The terrain of the study area is relatively flat, but micro-terrain features such as the northern mountainous region and the southern hills affect the formation, intensity, and spatial-temporal distribution of extreme rainfall to a certain degree by influencing atmospheric stability, wind fields, and water vapor transport, among other factors [90]. Mountains can affect the generation of extreme precipitation by lifting or blocking low-level airflow and inducing substantial rain when unstable airflow impacts the terrain [91,92]. Meanwhile, the terrain affects atmospheric water vapor transport, and upward airflow can cause convective precipitation, enhancing precipitation intensity. Rainshadow phenomena may occur near mountainous areas, resulting in less rainfall, and changes in wind direction in hilly areas may cause intense precipitation to concentrate in specific areas [93,94].

Human activities have led to global warming and increased tropical humidity, increasing precipitation in the H-Plain [95]. Human activities contribute more significantly than natural climate change to the variance in maximum daily rainfall (about 10%). Rapid economic development has occurred in the past 30 years [96]. Land use/cover change (LUCC) has an important influence on weather phenomena such as precipitation. Paddy fields, forests, and wetlands positively affect rainfall, as their centroids shift in the same direction as the precipitation centroid. Compared with other land use types, forests significantly impact increasing precipitation [97]. LUCC can significantly impact urban hydrological systems, leading to increased risks of urban rain and flood events by reducing the ability

of the system to regulate floods, known as urban flood regulation services (UFRS) for individual cities [98].

5. Conclusions

This study examines the temporal and spatial dynamics of daily and hourly extreme rainfall in the H-Plain between 1980 and 2020, compares and analyzes their differential characteristics, and explores the main factors affecting severe rainstorms at the hourly scale. The following conclusions are drawn:

(1) The H-Plain exhibits a decreasing trend in extreme daily rainfall and an increasing trend in intensity, with the Huaihe River region and the Shandong Peninsula being the highest-incidence areas, where extreme daily rainfall occurs in a more concentrated area and is likely to cause more serious disasters.

(2) Hourly extreme precipitation events have shown a significant increase in the Shandong and Henan regions of the H-Plain, while in the northwest of the Plain, they have shown a weakening trend.

(3) Hourly extreme rainfall events in the H-Plain typically occur frequently and in a discontinuous manner, with intensity gradually decreasing over time. The peak period of its occurrence is at night, mainly between 7 p.m. and 9 p.m. During the peak time of 19:00–21:00, the distribution of extreme rainfall indicates that the eastern region experiences more significant precipitation, intensity, and frequency, whereas the western region has lower levels of rain, power, and frequency.

(4) Hourly extreme rainfall events in the H-Plain have increased more than extreme daily events, and the rain type was mainly rear-type precipitation.

(5) Hourly extreme precipitation events in the H-Plain are greatly influenced by topography and LUCC. The micro-topography in hilly areas leads to a concentrated precipitation distribution, and LUCC suppresses extreme precipitation events under dry climates.

(6) The spatial distribution of the NDVI at the ten-day scale exhibits a gradually increasing trend from northwest to southeast, consistent with the pattern of extreme hourly precipitation. For extreme hourly precipitation, there is no significant change observed at the multi-year ten-day scale. The NDVI in the northern and central parts of the H-Plain shows a significant decreasing trend; in contrast, it presents a significant increasing trend in the southern region. Moreover, the correlation between extreme hourly rainfall and NDVI at the ten-day scale demonstrates distinct regional differentiation (almost all correlation coefficients pass the significance test), decreasing gradually from north to south. The lagged correlation analysis of extreme hourly precipitation and NDVI for one, two, and three ten-day periods shows that the lagged effect of extreme hourly precipitation on the NDVI is negligible. The correlation analysis of extreme hourly rainfall and NDVI for different months shows that extreme hourly precipitation negatively impacts NDVI.

Author Contributions: Conceptualization, H.Z. and Y.L.; methodology, Z.L.; data curation, H.Z. and Z.L.; software, H.Z.; validation, Y.L. and H.Z.; formal analysis, H.Z.; writing—original draft, H.Z.; writing—review and editing, Y.L. and H.Z. All authors have read and agreed to the published version of the manuscript.

Funding: This research was supported by the "The Nanjing Vocational University of Industry Technology's University-level Introduced Talent Research Start-up Fund Project (Natural Science Category) (YK21-05-07); in part by the Research Funds of Jiangsu Hydraulic Research Institute (2022z021); and in part by the research project "Research and Application of Reservoir Meteorological Risk Early Warning Technology Based on Deep Neural Networks" (GF21D050002) is funded by the Zhejiang Province Basic Public Welfare Research Program.

Acknowledgments: The authors are grateful to the editor and reviewers for their insightful suggestions and valuable assistance in enhancing the quality of the manuscript.

Conflicts of Interest: The authors declare no conflict of interest.

References

1. IPCC. *Climate Change 2021: The Physical Science Basis*; Cambridge University Press: Cambridge, UK, 2021.
2. Iyakaremye, V.; Zeng, G.; Zhang, G. Changes in extreme temperature events over Africa under 1.5 and 2.0 °C global warming scenarios. *Int. J. Climatol.* **2021**, *41*, 1506–1524. [CrossRef]
3. Wang, X.; Li, Y.; Wang, M.; Li, Y.; Gong, X.; Chen, Y.; Chen, Y.; Cao, W. Changes in daily extreme temperature and precipitation events in mainland China from 1960 to 2016 under global warming. *Int. J. Clim.* **2021**, *41*, 1465–1483. [CrossRef]
4. Li, C.; Zwiers, F.; Zhang, X.; Chen, G.; Lu, J.; Li, G.; Norris, J.; Tan, Y.; Sun, Y.; Liu, M. Larger Increases in More Extreme Local Precipitation Events as Climate Warms. *Geophys. Res. Lett.* **2019**, *46*, 6885–6891. [CrossRef]
5. Baldwin, J.W.; Dessy, J.B.; Vecchi, G.A.; Oppenheimer, M. Temporally Compound Heat Wave Events and Global Warming: An Emerging Hazard. *Earth's Future* **2019**, *7*, 411–427. [CrossRef]
6. Teshome, A.; Zhang, J. Increase of Extreme Drought over Ethiopia under Climate Warming. *Adv. Meteorol.* **2019**, *2019*, 5235429. [CrossRef]
7. Osburn, L.; Hope, P.; Dowdy, A. Changes in hourly extreme precipitation in Victoria, Australia, from the observational record. *Weather Clim. Extremes* **2021**, *31*, 100294. [CrossRef]
8. Myhre, G.; Alterskjær, K.; Stjern, C.W.; Hodnebrog, Ø.; Marelle, L.; Samset, B.H.; Sillmann, J.; Schaller, N.; Fischer, E.; Schulz, M.; et al. Frequency of extreme precipitation increases extensively with event rareness under global warming. *Sci. Rep.* **2019**, *9*, 16063. [CrossRef]
9. Li, J.; Wang, B. Predictability of summer extreme precipitation days over eastern China. *Clim. Dyn.* **2018**, *51*, 4543–4554. [CrossRef]
10. Liu, W.; Wu, J.; Tang, R.; Ye, M.; Yang, J. Daily Precipitation Threshold for Rainstorm and Flood Disaster in the Mainland of China: An Economic Loss Perspective. *Sustainability* **2020**, *12*, 407. [CrossRef]
11. Gu, X.; Ye, L.; Xin, Q.; Zhang, C.; Zeng, F.; Nerantzaki, S.D.; Papalexiou, S.M. Extreme Precipitation in China: A Review on Statistical Methods and Applications. *Adv. Water Resour.* **2022**, *163*, 104144. [CrossRef]
12. Su, Y.; Zhao, F.; Tan, L. Whether a large disaster could change public concern and risk perception: A case study of the 7/21 extraordinary rainstorm disaster in Beijing in 2012. *Nat. Hazards* **2015**, *78*, 555–567. [CrossRef]
13. Zhang, Q.; Zheng, Y.; Singh, V.P.; Luo, M.; Xie, Z. Summer extreme precipitation in eastern China: Mechanisms and impacts. *J. Geophys. Res. Atmos.* **2017**, *122*, 2766–2778. [CrossRef]
14. Zhang, J.; Gao, G.; Fu, B.; Wang, C.; Gupta, H.V.; Zhang, X.; Li, R. A universal multifractal approach to assessment of spatiotemporal extreme precipitation over the Loess Plateau of China. *Hydrol. Earth Syst. Sci.* **2020**, *24*, 809–826. [CrossRef]
15. Li, W.; He, X.; Scaioni, M.; Yao, D.; Mi, C.; Zhao, J.; Chen, Y.; Zhang, K.; Gao, J.; Li, X. Annual precipitation and daily extreme precipitation distribution: Possible trends from 1960 to 2010 in urban areas of China. *Geomat. Nat. Hazards Risk* **2019**, *10*, 1694–1711. [CrossRef]
16. Sun, W.; Mu, X.; Song, X.; Wu, D.; Cheng, A.; Qiu, B. Changes in extreme temperature and precipitation events in the Loess Plateau (China) during 1960–2013 under global warming. *Atmos. Res.* **2016**, *168*, 33–48. [CrossRef]
17. Lin, L.; Gao, T.; Luo, M.; Ge, E.; Yang, Y.; Liu, Z.; Zhao, Y.; Ning, G. Contribution of urbanization to the changes in extreme climate events in urban agglomerations across China. *Sci. Total Environ.* **2020**, *744*, 140264. [CrossRef]
18. Xu, H.; Chen, H.; Wang, H. Detectable Human Influence on Changes in Precipitation Extremes Across China. *Earth's Future* **2022**, *10*, e2021EF002409. [CrossRef]
19. Guo, X.; Wu, Z.; He, H.; Du, H.; Wang, L.; Yang, Y.; Zhao, W. Variations in the start, end, and length of extreme precipitation period across China. *Int. J. Climatol.* **2018**, *38*, 2423–2434. [CrossRef]
20. Wang, D.; Dong, Z.; Ling, Z.; Jiang, F.; Zhu, S.; Chen, J. Spatiotemporal variability of extreme precipitation at different time scales and quantitative analysis of associated driving teleconnection factors: Insights from Taihu Basin, China. *Ecol. Indic.* **2022**, *142*, 109287. [CrossRef]
21. Mou, Y.; Gao, X.; Yang, Z.; Xu, T.; Feng, J. Variation characteristics and the impact of urbanization of extreme precipitation in Shanghai. *Sci. Rep.* **2022**, *12*, 17618. [CrossRef]
22. Shahi, N.K.; Polcher, J.; Bastin, S.; Pennel, R.; Fita, L. Assessment of the spatio-temporal variability of the added value on precipitation of convection-permitting simulation over the Iberian Peninsula using the RegIPSL regional earth system model. *Clim. Dyn.* **2022**, *59*, 471–498. [CrossRef]
23. Mathbout, S.; Lopez-Bustins, J.A.; Royé, D.; Martin-Vide, J.; Benhamrouche, A. Spatiotemporal variability of daily precipitation concentration and its relationship to teleconnection patterns over the Mediterranean during 1975–2015. *Int. J. Climatol.* **2020**, *40*, 1435–1455. [CrossRef]
24. Wang, Q.; Zhang, M.; Wang, S.; Ma, Q.; Sun, M. Changes in temperature extremes in the Yangtze River Basin, 1962–2011. *J. Geogr. Sci.* **2014**, *24*, 59–75. [CrossRef]
25. Li, Y.-G.; He, D.; Hu, J.-M.; Cao, J. Variability of extreme precipitation over Yunnan Province, China 1960–2012. *Int. J. Climatol.* **2015**, *35*, 245–258. [CrossRef]
26. He, B.-R.; Zhai, P.-M. Changes in persistent and non-persistent extreme precipitation in China from 1961 to 2016. *Adv. Clim. Chang. Res.* **2018**, *9*, 177–184. [CrossRef]

27. Wang, B.; Zhang, M.; Wei, J.; Wang, S.; Li, X.; Li, S.; Zhao, A.; Li, X.; Fan, J. Changes in extreme precipitation over Northeast China, 1960–2011. *Quat. Int.* **2013**, *298*, 177–186. [CrossRef]
28. Guerreiro, S.B.; Fowler, H.J.; Barbero, R.; Westra, S.; Lenderink, G.; Blenkinsop, S.; Lewis, E.; Li, X.-F. Detection of continental-scale intensification of hourly rainfall extremes. *Nat. Clim. Chang.* **2018**, *8*, 803–807. [CrossRef]
29. Berg, P.M.V.D.; Moseley, C.; O Haerter, J. SStrong increase in convective precipitation in response to higher temperatures. *Nat. Geosci.* **2013**, *6*, 181–185. [CrossRef]
30. Soro, G.E.; Noufé, D.; Bi, T.A.G.; Shorohou, B. Trend Analysis for Extreme Rainfall at Sub-Daily and Daily Timescales in Côte d'Ivoire. *Climate* **2016**, *4*, 37. [CrossRef]
31. Alexander, L.V.; Fowler, H.J.; Bador, M.; Behrangi, A.; Donat, M.G.; Dunn, R.; Funk, C.; Goldie, J.; Lewis, E.; Rogé, M.; et al. On the use of indices to study extreme precipitation on sub-daily and daily timescales. *Environ. Res. Lett.* **2019**, *14*, 125008. [CrossRef]
32. Chinita, M.J.; Richardson, M.; Teixeira, J.; Miranda, P.M.A. Global mean frequency increases of daily and sub-daily heavy precipitation in ERA5. *Environ. Res. Lett.* **2021**, *16*, 074035. [CrossRef]
33. Ayat, H.; Evans, J.P.; Sherwood, S.C.; Soderholm, J. Intensification of subhourly heavy rainfall. *Science* **2022**, *378*, 655–659. [CrossRef] [PubMed]
34. Yu, L.; Zhong, S.; Pei, L.; Bian, X.; Heilman, W.E. Contribution of large-scale circulation anomalies to changes in extreme precipitation frequency in the United States. *Environ. Res. Lett.* **2016**, *11*, 044003. [CrossRef]
35. Barbero, R.; Fowler, H.J.; Lenderink, G.; Blenkinsop, S. Is the intensification of precipitation extremes with global warming better detected at hourly than daily resolutions? *Geophys. Res. Lett.* **2017**, *44*, 974–983. [CrossRef]
36. Lenderink, G.; Barbero, R.; Loriaux, J.M.; Fowler, H.J. Super-Clausius–Clapeyron Scaling of Extreme Hourly Convective Precipitation and Its Relation to Large-Scale Atmospheric Conditions. *J. Clim.* **2017**, *30*, 6037–6052. [CrossRef]
37. Wang, J.; Chen, F.; Doan, Q.-V.; Xu, Y. Exploring the effect of urbanization on hourly extreme rainfall over Yangtze River Delta of China. *Urban Clim.* **2021**, *36*, 100781. [CrossRef]
38. Formetta, G.; Marra, F.; Dallan, E.; Zaramella, M.; Borga, M. Differential orographic impact on sub-hourly, hourly, and daily extreme precipitation. *Adv. Water Resour.* **2022**, *159*, 104085. [CrossRef]
39. Yin, J.; Yan, D.; Yang, Z.; Yuan, Z.; Yuan, Y.; Zhang, C. Projection of extreme precipitation in the context of climate change in Huang-Huai-Hai region, China. *J. Earth Syst. Sci.* **2016**, *125*, 417–429. [CrossRef]
40. Zhang, D.-D.; Yan, D.-H.; Wang, Y.-C.; Lu, F.; Wu, D. Changes in extreme precipitation in the Huang-Huai-Hai River basin of China during 1960–2010. *Theor. Appl. Climatol.* **2015**, *120*, 195–209. [CrossRef]
41. Yuan, Y.; Yan, D.; Yuan, Z.; Yin, J.; Zhao, Z. Spatial Distribution of Precipitation in Huang-Huai-Hai River Basin between 1961 to 2016, China. *Int. J. Environ. Res. Public Health* **2019**, *16*, 3404. [CrossRef]
42. Christensen, J.H.; Christensen, O.B. Severe summertime flooding in Europe. *Nature* **2003**, *421*, 805–806. [CrossRef] [PubMed]
43. Hanel, M.; Buishand, T.A. Analysis of precipitation extremes in an ensemble of transient regional climate model simulations for the Rhine basin. *Clim. Dyn.* **2011**, *36*, 1135–1153. [CrossRef]
44. Westra, S.; Fowler, H.J.; Evans, J.P.; Alexander, L.V.; Berg, P.; Johnson, F.; Kendon, E.J.; Lenderink, G.; Roberts, N.M. Future changes to the intensity and frequency of short-duration extreme rainfall. *Rev. Geophys.* **2014**, *52*, 522–555. [CrossRef]
45. Li, J.; Yu, R.; Sun, W. Duration and seasonality of hourly extreme rainfall in the central eastern China. *Acta Meteorol. Sin.* **2013**, *27*, 799–807. [CrossRef]
46. Trenberth, K.E.; Dai, A.; Rasmussen, R.M.; Parsons, D.B. The Changing Character of Precipitation. *Bull. Am. Meteorol. Soc.* **2003**, *84*, 1205–1218. [CrossRef]
47. Tabari, H. Climate change impact on flood and extreme precipitation increases with water availability. *Sci. Rep.* **2020**, *10*, 13768. [CrossRef]
48. Sridhar, V.; Modi, P.; Billah, M.M.; Valayamkunnath, P.; Goodall, J.L. Precipitation Extremes and Flood Frequency in a Changing Climate in Southeastern Virginia. *JAWRA J. Am. Water Resour. Assoc.* **2019**, *55*, 780–799. [CrossRef]
49. Yuan, W.; Yu, R.; Zhang, M.; Lin, W.; Chen, H.; Li, J. Regimes of Diurnal Variation of Summer Rainfall over Subtropical East Asia. *J. Clim.* **2012**, *25*, 3307–3320. [CrossRef]
50. Smith, T.M.; Reynolds, R.W.; Peterson, T.C.; Lawrimore, J. Improvements to NOAA's Historical Merged Land–Ocean Surface Temperature Analysis (1880–2006). *J. Clim.* **2008**, *21*, 2283–2296. [CrossRef]
51. Hong, Y.; Hsu, K.-L.; Sorooshian, S.; Gao, X. Precipitation Estimation from Remotely Sensed Imagery Using an Artificial Neural Network Cloud Classification System. *J. Appl. Meteorol.* **2004**, *43*, 1834–1853. [CrossRef]
52. Adler, R.; Gu, G.; Sapiano, M.; Wang, J.-J.; Huffman, G. Global Precipitation: Means, Variations and Trends During the Satellite Era (1979–2014). *Surv. Geophys.* **2017**, *38*, 679–699. [CrossRef]
53. Tabari, H. Extreme value analysis dilemma for climate change impact assessment on global flood and extreme precipitation. *J. Hydrol.* **2021**, *593*, 125932. [CrossRef]
54. Dee, D.P.; Uppala, S.M.; Simmons, A.J.; Berrisford, P.; Poli, P.; Kobayashi, S.; Andrae, U.; Balmaseda, M.A.; Balsamo, G.; Bauer, P.; et al. The ERA-Interim reanalysis: Configuration and performance of the data assimilation system. *Q. J. R. Meteorol. Soc.* **2011**, *137*, 553–597. [CrossRef]
55. Sharma, A.; Wasko, C.; Lettenmaier, D.P. If Precipitation Extremes Are Increasing, Why Aren't Floods? *Water Resour. Res.* **2018**, *54*, 8545–8551. [CrossRef]

56. Hu, Z.; Wu, Z.; Islam, A.R.M.T.; You, X.; Liu, C.; Li, Q.; Zhang, X. Spatiotemporal characteristics and risk assessment of agricultural drought disasters during the winter wheat-growing season on the Huang-Huai-Hai Plain, China. *Theor. Appl. Climatol.* **2021**, *143*, 1393–1407. [CrossRef]
57. Stoyanova, J.S.; Georgiev, C.G.; Neytchev, P.N. Drought Monitoring in Terms of Evapotranspiration Based on Satellite Data from Meteosat in Areas of Strong Land– Atmosphere Coupling. *Land* **2023**, *12*, 240.
58. Ren, F.; Wu, G.; Dong, W.; Wang, X.; Wang, Y.; Ai, W.; Li, W. Changes in tropical cyclone precipitation over China. *Geophys. Res. Lett.* **2006**, *33*. [CrossRef]
59. Jiang, P.; Yu, Z.; Yuan, F.; Acharya, K. The Multi-Scale Temporal Variability of Extreme Precipitation in the Source Region of the Yellow River. *Water* **2019**, *11*, 92. [CrossRef]
60. Li, Y.; Huang, H.; Ju, H.; Lin, E.; Xiong, W.; Han, X.; Wang, H.; Peng, Z.; Wang, Y.; Xu, J.; et al. Assessing vulnerability and adaptive capacity to potential drought for winter-wheat under the RCP 8.5 scenario in the Huang-Huai-Hai Plain. *Agric. Ecosyst. Environ.* **2015**, *209*, 125–131. [CrossRef]
61. Xiao, D.; Shen, Y.; Qi, Y.; Moiwo, J.P.; Min, L.; Zhang, Y.; Guo, Y.; Pei, H. Impact of alternative cropping systems on groundwater use and grain yields in the North China Plain Region. *Agric. Syst.* **2017**, *153*, 109–117. [CrossRef]
62. Yang, J.; Huang, M.; Zhai, P. Performance of the CRA-40/Land, CMFD, and ERA-Interim Datasets in Reflecting Changes in Surface Air Temperature over the Tibetan Plateau. *J. Meteorol. Res.* **2021**, *35*, 663–672. [CrossRef]
63. Jin, H.; Chen, X.; Zhong, R.; Pan, Y.; Zhao, T.; Liu, Z.; Tu, X. Corrected GCM data through CMFD data to analysis future runoff changes in the source region of the Yangtze River, China. *Environ. Earth Sci.* **2022**, *81*, 527. [CrossRef]
64. Li, H.; Wang, X.; Choy, S.; Jiang, C.; Wu, S.; Zhang, J.; Qiu, C.; Zhou, K.; Li, L.; Fu, E.; et al. Detecting heavy rainfall using anomaly-based percentile thresholds of predictors derived from GNSS-PWV. *Atmos. Res.* **2022**, *265*, 105912. [CrossRef]
65. Holben, B.N. Characteristics of maximum-value composite images from temporal AVHRR data. *Int. J. Remote Sens.* **1986**, *7*, 1417–1434. [CrossRef]
66. Zhu, Y.; Liu, X.; Zhang, Y.; Chen, C.; Shen, L.; Ju, Q.; Zhou, T.; Xia, P. The Proportional Characteristics of Daytime and Nighttime Precipitation Based on Daily Precipitation in Huai River Basin, China. *Atmosphere* **2022**, *13*, 1287. [CrossRef]
67. Li, Y.; Ren, G.; Wang, Q.; You, Q. More extreme marine heatwaves in the China Seas during the global warming hiatus. *Environ. Res. Lett.* **2019**, *14*, 104010. [CrossRef]
68. Li, D.; Sun, J.; Fu, S.; Wei, J.; Wang, S.; Tian, F. Spatiotemporal characteristics of hourly precipitation over central eastern China during the warm season of 1982–2012. *Int. J. Climatol.* **2016**, *36*, 3148–3160. [CrossRef]
69. Tao, Y.; Wang, W.; Song, S.; Ma, J. Spatial and Temporal Variations of Precipitation Extremes and Seasonality over China from 1961~2013. *Water* **2018**, *10*, 719. [CrossRef]
70. Li, X.; Zhang, K.; Bao, H.; Zhang, H. Climatology and changes in hourly precipitation extremes over China during 1970–2018. *Sci. Total. Environ.* **2022**, *839*, 156297. [CrossRef]
71. Zhang, W.; Jin, F.-F.; Turner, A. Increasing autumn drought over southern China associated with ENSO regime shift. *Geophys. Res. Lett.* **2014**, *41*, 4020–4026. [CrossRef]
72. Wu, Z.; Huang, N.E.; Wallace, J.M.; Smoliak, B.V.; Chen, X. On the time-varying trend in global-mean surface temperature. *Clim. Dyn.* **2011**, *37*, 759–773. [CrossRef]
73. Zhang, P.; Liu, Y.; He, B. Impact of East Asian Summer Monsoon Heating on the Interannual Variation of the South Asian High. *J. Clim.* **2016**, *29*, 159–173. [CrossRef]
74. Freychet, N.; Hsu, H.-H.; Chou, C.; Wu, C.-H. Asian Summer Monsoon in CMIP5 Projections: A Link between the Change in Extreme Precipitation and Monsoon Dynamics. *J. Clim.* **2015**, *28*, 1477–1493. [CrossRef]
75. Wang, B.; Wu, R.; Lau, K.M. Interannual Variability of the Asian Summer Monsoon: Contrasts between the Indian and the Western North Pacific–East Asian Monsoons. *J. Clim.* **2001**, *14*, 4073–4090. [CrossRef]
76. Chen, S.; Kang, Z.; Liu, M.; Lv, R.; Ma, J.; He, J. Subseasonal Variation of 2020 Meiyu Rainfall With Extremely Long Duration Over the Yangtze–Huaihe River Basin in China. *Front. Earth Sci.* **2022**, *9*, 946252. [CrossRef]
77. Lu, W.; Zhu, Y.; Ha, Y.; Zhong, Z.; Hu, Y. Recent Decadal Weakening of the Summertime Rainfall Interannual Variability Over Yellow-Huaihe River Valley Attributable to the Western Pacific Cooling. *Front. Earth Sci.* **2022**, *10*, 946252. [CrossRef]
78. Jiang, F.; Zhang, W.; Geng, X.; Stuecker, M.F.; Liu, C. Impacts of Central Pacific El Niño on Southern China Spring Precipitation Controlled by its Longitudinal Position. *J. Clim.* **2019**, *32*, 7823–7836. [CrossRef]
79. Hu, K.; Xie, S.-P.; Huang, G. Orographically Anchored El Niño Effect on Summer Rainfall in Central China. *J. Clim.* **2017**, *30*, 10037–10045. [CrossRef]
80. YDing, Y.; Liu, Y.; Liang, S.; Ma, X.; Zhang, Y.; Si, D.; Liang, P.; Song, Y.; Zhang, J. Interdecadal Variability of the East Asian Winter Monsoon and Its Possible Links to Global Climate Change. *J. Meteorol. Res.* **2014**, *28*, 693–713. [CrossRef]
81. Gu, W.; Chen, L.-J.; Wang, Y.-G.; Gao, H.; Wang, L.; Liu, Y.-Y. Extreme precipitation over northern China in autumn 2021 and joint contributions of tropical and mid-latitude factors. *Adv. Clim. Chang. Res.* **2022**, *13*, 835–842. [CrossRef]
82. Yang, K.; Cai, W.; Huang, G.; Hu, K.; Ng, B.; Wang, G. Increased variability of the western Pacific subtropical high under greenhouse warming. *Proc. Natl. Acad. Sci. USA* **2022**, *119*, e2120335119. [CrossRef]
83. Song, X.; Zou, X.; Zhang, C.; Zhang, J.; Kong, F. Multiscale Spatio-Temporal Changes of Precipitation Extremes in Beijing-Tianjin-Hebei Region, China during 1958–2017. *Atmosphere* **2019**, *10*, 462. [CrossRef]

84. Zheng, Y.; Xue, M.; Li, B.; Chen, J.; Tao, Z. Spatial characteristics of extreme rainfall over China with hourly through 24-hour accumulation periods based on national-level hourly rain gauge data. *Adv. Atmos. Sci.* **2016**, *33*, 1218–1232. [CrossRef]
85. Lu, Y.; Jiang, S.; Ren, L.; Zhang, L.; Wang, M.; Liu, R.; Wei, L. Spatial and Temporal Variability in Precipitation Concentration over Mainland China, 1961–2017. *Water* **2019**, *11*, 881. [CrossRef]
86. Ling, M.; Han, H.; Wei, X.; Lv, C. Temporal and spatial distributions of precipitation on the Huang-Huai-Hai Plain during 1960–2019, China. *J. Water Clim. Chang.* **2021**, *12*, 2232–2244. [CrossRef]
87. Ling, M.; Han, H.; Yu, L.; Tang, S. Precipitation barycenter and relationship to the spatial distribution of station networks on the Huang-Huai-Hai Plain, China. *J. Water Clim. Chang.* **2021**, *12*, 3839–3850. [CrossRef]
88. Li, J.; Li, N.; Yu, R. Regional Differences in Hourly Precipitation Characteristics along the Western Coast of South China. *J. Appl. Meteorol. Climatol.* **2019**, *58*, 2717–2732. [CrossRef]
89. Hu, C.; Fung, K.Y.; Tam, C.; Wang, Z.; Chenxi, H.; Ziqian, W. Urbanization Impacts on Pearl River Delta Extreme Rainfall Sensitivity to Land Cover Change Versus Anthropogenic Heat. *Earth Space Sci.* **2021**, *8*, e2020EA001536. [CrossRef]
90. Ren, M.; Xu, Z.; Pang, B.; Liu, J.; Du, L. Spatiotemporal Variability of Precipitation in Beijing, China during the Wet Seasons. *Water* **2020**, *12*, 716. [CrossRef]
91. Cui, F.; Hamdi, R.; He, H.; Yuan, X.; Yang, T.; Tang, H.; Wang, B.; Zhang, Q.; Termonia, P.; De Maeyer, P. Interplay Between Urbanization and Irrigation on Summer Climate in the Huang-Huai-Hai Plain, China. *J. Geophys. Res. Atmos.* **2022**, *127*, e2021JD036053. [CrossRef]
92. Kim, Y.-J.; Jee, J.-B.; Lim, B. Investigating the Influence of Water Vapor on Heavy Rainfall Events in the Southern Korean Peninsula. *Remote Sens.* **2023**, *15*, 340. [CrossRef]
93. Lu, F.; Lu, H. A high-resolution grid dataset of air temperature and precipitation for Qinling-Daba Mountains in central China and its implications for regional climate. *ACTA Geogr. Sin.* **2019**, *74*, 875–888. [CrossRef]
94. Wang, L.; Chen, S.; Zhu, W.; Ren, H.; Zhang, L.; Zhu, L. Spatiotemporal variations of extreme precipitation and its potential driving factors in China's North-South Transition Zone during 1960–2017. *Atmos. Res.* **2021**, *252*, 105429. [CrossRef]
95. Zhu, D.; Zhi, X.; Wang, N.; Chen, C.; Tian, X.; Yu, Y. Impacts of Changbai Mountain Topography on the Extreme Precipitation From Super Typhoon Maysak. *Front. Environ. Sci.* **2022**, *9*, 818402. [CrossRef]
96. Zhao, Y.; Chen, D.; Li, J.; Chen, D.; Chang, Y.; Li, J.; Qin, R. Enhancement of the summer extreme precipitation over North China by interactions between moisture convergence and topographic settings. *Clim. Dyn.* **2020**, *54*, 2713–2730. [CrossRef]
97. Knutson, T.; Camargo, S.J.; Chan, J.C.L.; Emanuel, K.; Ho, C.-H.; Kossin, J.; Mohapatra, M.; Satoh, M.; Sugi, M.; Walsh, K.; et al. Tropical Cyclones and Climate Change Assessment: Part II: Projected Response to Anthropogenic Warming. *Bull. Am. Meteorol. Soc.* **2020**, *101*, E303–E322. [CrossRef]
98. Gao, L.; Huang, J.; Chen, X.; Chen, Y.; Liu, M. Contributions of natural climate changes and human activities to the trend of extreme precipitation. *Atmos. Res.* **2018**, *205*, 60–69. [CrossRef]